

MODELING AND OPTIMIZATION OF SYSTEMS FOR NUTRIENT RECOVERY FROM LIVESTOCK WASTE

EDGAR MARTÍN HERNÁNDEZ

A dissertation submitted for the degree of
DOCTOR IN CHEMICAL SCIENCE AND TECHNOLOGY

at the
UNIVERSIDAD DE SALAMANCA



VNiVERSiDAD
DE SALAMANCA

CAMPUS OF INTERNATIONAL EXCELLENCE

Academic advisor: Mariano Martín Martín

Programa de Doctorado en Ciencia y Teconología Química

Departamento de Ingeniería Química y Textil

Universidad de Salamanca

March 2022

A mi familia, y a todos los que por mi vida pasaron.

*No tenemos un tiempo escaso, sino que perdemos mucho.
La vida es lo bastante larga para realizar las mayores empresas,
pero si se desparrama en la ostentación y la dejadez,
donde no se gasta en nada bueno, cuando al final
nos acosa el inevitable trance final, nos damos cuenta
de que ha pasado una vida que no supimos que estaba pasando.*

— Séneca, De la brevedad de la vida.

ACKNOWLEDGMENTS

Complete

ABSTRACT

To be completed.

RESUMEN

Completar.

PUBLICATIONS

This thesis is presented as a compendium of publications, where each of the chapters corresponds to a formal manuscript published in a scientific journal, or currently under review, and book chapters. The relation of manuscripts published or under review, and book chapters that comprise this dissertation is detailed below:

- [1] E. Martín-Hernández, L.S. Guerras, and M. Martín. «Optimal technology selection for the biogas upgrading to biomethane.» In: *Journal of Cleaner Production* (2020), p. 122032.
- [2] E. Martín-Hernández, Y. Hu, V.M. Zavala, M. Martín, and G.J. Ruiz-Mercado. «Analysis of incentive policies for phosphorus recovery at livestock facilities in the Great Lakes area.» In: *Resources, Conservation & Recycling* (Under Review).
- [3] E. Martín-Hernández, M. Martín, and G.J. Ruiz-Mercado. «A geospatial environmental and techno-economic framework for sustainable phosphorus management at livestock facilities.» In: *Resources, Conservation & Recycling* (Under Review).
- [4] E. Martín-Hernández, G.J. Ruiz-Mercado, and M. Martín. «Model-driven spatial evaluation of nutrient recovery from livestock leachate for struvite production.» In: *Journal of Environmental Management* 271 (2020), p. 110967.
- [5] E. Martín-Hernández, A.M. Sampat, M. Martin, V.M. Zavala, and G.J. Ruiz-Mercado. «A Logistics Analysis for Advancing Carbon and Nutrient Recovery from Organic Waste.» In: *Advances in Carbon Management Technologies*. CRC Press, 2021, pp. 186–207.
- [6] E. Martín-Hernández, A.M. Sampat, V.M. Zavala, and M. Martín. «Optimal integrated facility for waste processing.» In: *Chemical Engineering Research and Design* 131 (2018), pp. 160–182.
- [7] M. Mohammadi, E. Martín Hernández, M. Martín, and I. Harjunkoski. «Modeling and Analysis of Organic Waste Management Systems in Centralized and Decentralized Supply Chains Using Generalized Disjunctive Programming.» In: *Industrial & Engineering Chemistry Research* 60.4 (2021), pp. 1719–1745.

CONTENTS

1 INTRODUCTION	1
I PHOSPHORUS MANAGEMENT	
2 ASSESSMENT OF PHOSPHORUS RECOVERY THROUGH STRUVITE PRECIPITATION	5
2.1 Introduction	5
2.2 Methods	7
2.2.1 Spatial resolution	7
2.2.2 Assessment of anthropogenic phosphorus from agricultural activities	8
2.2.3 Thermodynamic model for precipitates formation	9
2.3 Results and discussion	17
2.3.1 Surrogate models to estimate the formation of precipitates from livestock organic waste	17
2.3.2 Phosphorus releases from cattle leachate potentially avoided via struvite formation	21
2.4 Conclusions	25
Nomenclature	26
Acknowledgments	27
Bibliography	27
II APPENDIX	
A APPENDIX A: SUPPLEMENTARY INFORMATION OF CHAPTER 2	35
A.1 Biogas production	35
A.2 H₂S removal	38
A.3 CO₂, NH₃ and H₂O removal (PSA)	39
A.4 Brayton cycle	39
A.5 Rankine cycle	40
Bibliography	42
B APPENDIX B: SUPPLEMENTARY INFORMATION OF CHAPTER 3	45
B.1 Cattle organic waste composition	45
B.2 Distribution functions of elements from cattle waste	48
B.3 Thermodynamic modeling of the carbonates system	50
B.4 Surrogate models to estimate the formation of precipitates from livestock organic waste	53
B.4.1 Influence of magnesium	53
Bibliography	54
C APPENDIX C: SUPPLEMENTARY INFORMATION OF CHAPTER 4	61
C.1 Biogas production	61

D APPENDIX D: SUPPLEMENTARY INFORMATION OF CHAPTER 6	63
D.1 Biogas production	63
E APPENDIX E: SUPPLEMENTARY INFORMATION OF CHAPTER 7	65
E.1 Literature review	65
E.2 Modelling approach	65
E.2.1 Amines	65
E.2.2 PSA	68
E.2.3 Membranes	71
E.3 Economic evaluation	73
E.4 Scaling-up study	74
Bibliography	75

LIST OF FIGURES

Figure 2.1	Flowchart of the proposed algorithm to solve the thermodynamic model for the formation of precipitates in cattle organic waste.	15
Figure 2.2	A solution procedure to evaluate the influence of the cattle waste composition variability in the formation of struvite.	16
Figure 2.3	Comparison between experimental results reported by Zeng and Li [53] and the results provided by the model developed in this work.	16
Figure 2.4	Influence of magnesium and calcium in struvite precipitation.	20
Figure 2.5	Techno-ecological synergy (TES) metric values for HUC8 watersheds. Red indicates watersheds with unbalanced agricultural phosphorus releases, and blue indicates watersheds with balanced agricultural phosphorus releases. White indicates watersheds with not available data.	22
Figure 2.6	Phosphorus releases avoided through struvite production for the different scenarios considered. Darker colors represent larger phosphorus recovery	23
Figure B.1	Kernel density estimation (red dashed line) and probability density distribution (blue solid line) for the evaluated components in cattle organic waste.	48
Figure B.2	Evolution phosphorus as phosphate fraction recovered as struvite and calcium fraction recovered as precipitates along Mg^{2+}/PO_4^{3-} molar ratio values considering 50 different composition data sets.	57
Figure B.3	Evolution of phosphorus as phosphate fraction recovered as struvite and calcium fraction recovered as precipitates along Ca^{2+}/PO_4^{3-} molar ratio values considering 50 different composition data sets.	58
Figure B.4	Evolution of phosphorus as phosphate fraction recovered as struvite and calcium fraction recovered as precipitates among alkalinity values considering 50 different composition data sets.	59

Figure E.1	Scheme of the proposed superstructure for bio-gas upgrading into biomethane.	66
------------	--	----

ACRONYMS

1

INTRODUCTION

To be completed

Part I

PHOSPHORUS MANAGEMENT

Complete introduction of Part I

2

ASSESSMENT OF PHOSPHORUS RECOVERY THROUGH STRUVITE PRECIPITATION

2.1 INTRODUCTION

Livestock farming and other agricultural activities have altered the natural nutrient cycles. Phosphorus, one of the three plant-grow macronutrients, enters to the global cycle as phosphate rock, which through erosion and chemical weathering is transferred to soils and waterbodies. Also, phosphorus deposited in soils will reach fresh and marine waterbodies by runoff. Phosphorus in rivers is transported to stagnant waterbodies (such as lakes) and oceans, reaching the bottom of lakes and oceans as sediments. The cycle is closed when the buried phosphorus is uplifted again by tectonic processes. Along the cycle, phosphorus can be taken by plants and algae, but after the death of living organisms it returns to the cycle [35]. This global natural cycle is largely altered by human activities through the mining and shipping of phosphate rock, mainly for fertilizer production, resulting in unbalanced phosphorus releases to the environment.

Nutrient pollution from anthropogenic sources has become as a critical worldwide water quality problems. Nutrient contamination results in environmental and public health issues as a result of the exponential growth of algae, cyanobacteria, and the occurrence of harmful algal blooms (HABs), which turns into dead zones and hypoxia due to the aerobic degradation of the algal biomass by bacteria; shifting the distribution of aquatic species and releasing toxins in drinking water [38]. In addition, the development of HABs and eutrophication processes contributes to climate change through the emission of large amounts of strong greenhouse gases such as CH₄ and N₂O [5].

However, phosphorus is a limited non-renewable resource, essential nutrient to support life, and widely used as fertilizer to increase crop yields. Actually, phosphorus is one of the most sensitive elements to depletion, as it is a key agricultural fertilizer that has no known substitute. Current global reserves of phosphate rock could be depleted in the next 50 to 100 years [9]. Therefore, the development of a circular economy around phosphorus capable of recovering the nutrient and reintegrating it into the productive cycle is not only desirable but also a necessary measure to reach sustainable development. Agricultural activities are the main source of nutrients in waterbodies [11], and among them, livestock industry is one of the largest economic sectors. Additionally, the increasing income-spending potential of the middle class in developing countries has increased the demand for dairy and

beef products, resulting in the generation of large amounts of livestock organic waste. Considering that an average dairy cow generates 51.19 kg of raw manure per day [48], the total phosphorus excreted is 11.02 kg per year per animal, equivalent to 5.96 kg of phosphorus as phosphate per year per animal. In the U.S. as of January 2020, a total of 94.4 million head has been reported [50]. Thus, this shows potential phosphate U.S. releases of $562.6 \cdot 10^6$ kg/yr. Sampat et al. [37] presented the link between the presence of livestock facilities and larger concentrations of phosphorus in soil, which potentially can be lost as runoff reaching waterbodies. For animals on pasture, organic waste should not be a resource of concern if stocking rates are not excessive. However, for concentrate animal feeding operations (CAFOs), manure should be correctly managed due to the high rates and spatial concentration of the organic waste generated, representing potential environmental issues. Usually, manure is collected in the animal living zones, and stored as liquid or slurry to be further spread in croplands as nutrient supplementation; or as solid in dry stacking or composting facilities to be sold as compost. Liquid fraction of manure can be also treated in aerobic or anaerobic ponds. However, these approaches do not allow a correct nutrient management since nutrients concentration is variable and not well defined, and nitrogen and phosphorus are unbalanced regarding the nutrient necessities of plants, i.e., if nitrogen demand is covered, there is a surplus in the phosphorus supply which can runoff to waterbodies, and if phosphorus demand is covered, there is a deficit in the nitrogen supply, being necessary to apply additional fertilizers. In addition, during rainy periods the applied manure can runoff, dragging the nutrients contained in it. Nonetheless, phosphorus from liquid cattle waste, either processed in an anaerobic digestion stage or raw waste, can be potentially recovered through different processes [26], reducing the nutrient inputs to waterbodies and its consequential environmental, economic, and social impacts. Among these, it is found that struvite production is one of the most promising cost-effective choices for the recovery of nutrients from cattle waste [22]. Struvite is a phosphate-based mineral, which can be applied as a slow release fertilizer [32], allowing the redistribution of phosphorus from livestock facilities to nutrient-deficient locations.

Previous studies report struvite formation from different sources of waste, such as municipal wastewater treatment plants [4], mineral fertilizer industry [23], or agricultural industry [40]. Thermodynamic models representing the formation of struvite and other precipitates have been also developed for various wastes including liquid swine manure [8], human urine [15, 33], and municipal wastewater [31]. Additionally, some complex approaches considering the hydrodynamic and kinetic effects in the formation of struvite have been studied but limited to wastewater treatment [21, 31]. However, the results obtained from those studies cannot be extrapolated to struvite formation from

cattle organic waste, since these residues have some characteristics that hinder struvite formation, including high ionic strength, which reduces the effective concentration of ions; the presence of calcium ions competing for phosphate ions [52], which inhibits a selective recovery by nutrient precipitation techniques; and the high variability in the manure composition, as a function of the geographical area, the animal feed, etc. [43]. Other controlling factors are the pH level, the magnesium-phosphorus ratio, and the alkalinity of the leachate. Therefore, for an accurate prediction of struvite formation from this waste, it is necessary to include within the thermodynamic model structure for precipitates formation the specific features of cattle waste described above.

In this work, specific surrogate models to predict the production of struvite and calcium precipitates from cattle leachate are developed based on a detailed and robust thermodynamic model. In addition, the variability in the organic waste composition is captured through a probability framework based on Monte Carlo method. The reduced models obtained are used to evaluate the potential of struvite production from cattle waste to mitigate phosphorus releases in watersheds of the United States. Future applications of the developed surrogate models include the development of applications for environmental assessment and the design of policies to prevent nutrient releases, among others.

2.2 METHODS

2.2.1 *Spatial resolution*

A watershed is an area of land which drains all the streams and rainfall to a common drainage, defining the spatial boundaries for the collection of lost elements as runoff. The surface water drainages of the U.S. are identified by the U.S. Geological Survey through the Hydrologic Unit Code system (HUC). The HUC system is a hierarchical system indicated by the number of digits in groups of two, with six levels identified by codes from 2 to 12 digits (i.e., HUC₂ to HUC₁₂). These levels refer to regions, subregions, basins, subbasins, watersheds, and subwatersheds. The spatial resolution of this study is the continental United States at watershed scale, considering the boundaries defined by the Hydrologic Unit Code system at 8 digits (HUC₈), representing the subbasin level [46].

2.2.2 Assessment of anthropogenic phosphorus from agricultural activities

2.2.2.1 Phosphorus releases

Agricultural emissions are one of the main sources of anthropogenic P releases due to the excessive use of commercial fertilizers and live-stock manure for cropland nutrients needs and the uncontrolled nutrient runoff to waterbodies, although for some areas urban source releases can contribute significantly to the total P releases to the environment. However, this analysis is limited to the evaluation of phosphorus releases from agricultural activities [1, 11, 42].

Watershed phosphorus releases (E_x) are computed as the sum of the phosphorus releases from fertilizer applications to croplands and from the manure generated by livestock facilities. The releases of phosphorus to each watershed by manure emissions, accounting cattle, swine and poultry, and by fertilizers application, is reported by the IPNI NuGIS project. This is consistent with the most recent data available (year 2014) for fertilizers sales provided by the Association of American Plant Food Control Officials (AAPFCO), fitting the data to HUC8 watershed boundaries. More information about the methodology used for the estimation of agricultural phosphorus releases can be found in [19]. Phosphorus content for several commercial phosphate fertilizers and different manure types can be found in Ohio State University Extension [28] and Ohio State University Extension [27] respectively.

2.2.2.2 Phosphorus uptakes

The elements considered for phosphorus uptake are the crops sown and managed by humans in each watershed. Additionally, the phosphorus retained by wetlands has been considered in the phosphorus balance. The phosphorus uptake by each type of vegetation at watershed level is computed as the product of the land area occupied, the grow yields per area unit and the phosphorus uptake per plant mass unit. Therefore, the total watershed phosphorus uptake (U_x) is computed as the sum of the phosphorus uptake by each type of plant, Eq. 2.1.

$$U_x = \sum^i \text{Area}_i \cdot \text{Yield}_i \cdot P_{\text{uptake}}_i \quad \forall i \in \text{Plant varieties} \quad (2.1)$$

Since different crops have different phosphorus uptakes and yield rates, the amount of each type of crop is estimated for each watershed. To determine the land cover uses, accounting croplands, pasturelands, wetlands and developed areas (urban areas), information available for the most recent year (2011) from the U.S. Environmental Protection Agency's (U.S. EPA) EnviroAtlas database is used [30]. Data from EnviroAtlas is provided with higher spatial resolution, at HUC12 level. To ensure spatial consistency, the data is reconciled at HUC8 level.

Once the land uses of each watershed are known, data from the 2017 U.S. Census of Agriculture is used to determine the distribution of crops on croplands, considering corn, soybeans, small grains, cotton, rice, vegetables, orchards, greenhouse and other crops (namely oil crops, sugar crops, and fruits) [49]. The data provided by the U.S. Census of Agriculture have a spatial resolution of HUC6. Therefore, it is reconciled at HUC8 level scaling by the area fraction represented by each HUC8 watershed over the total HUC6 hydrologic unit. If two or more crops were harvested from the same land during the year (double cropping), the area was counted for each crop. To determine the nutrients uptake of each type of crop, data from the U.S. Department of Agriculture (USDA) Waste Management field Handbook is considered [48]. For croplands, the specific nutrient uptake values are used for corn, soybeans, cotton, rice and orchards, while average values including the most representative species are used for small grains, vegetables, greenhouse crops, pasture crops, and forest. For pasture lands the average nutrient uptake and crop yield including the main pasture crops: alfalfa, switchgrass and wheatgrass; for forests lands the nutrient uptake and crop yield of Northern hardwoods is considered, and for developed areas null nutrient uptake is considered. The wetlands phosphorus uptake value considered is $0.77 \text{ gP m}^{-2} \text{ year}^{-1}$, based in the data reported by Kadlec [20].

2.2.2.3 *Phosphorus balance*

To reach environmental sustainability of a productive activity, the releases of phosphorus should be balanced with the phosphorus uptakes from that activity, reducing the impact over the original ecosystems as much as possible. To evaluate the balance of phosphorus releases involved in agricultural activities throughout the U.S. watersheds, the techno-ecological synergy (TES) sustainability metric proposed by Bakshi, Ziv, and Lepech [2] has been considered, Eq. 2.2. A negative value of V_x indicates that the emissions, (E_x), are larger than the uptake capacity of the agricultural activities, (U_x), impacting the ecosystems, while positive values reflect that the releases are lower than the uptake capacity.

$$V_x = \frac{(U_x - E_x)}{E_x} \quad (2.2)$$

2.2.3 *Thermodynamic model for precipitates formation*

The behavior of cattle leachate system has been evaluated through a thermodynamic model, evaluating the formation of different precipitates through chemical equilibrium and material balances, capturing the mutual dependencies based on the competition for the same

ions. Four aqueous chemical systems have been considered, water, ammonium, phosphoric acid, and carbonates systems. Moreover, the formation of seven possible precipitates is evaluated: struvite, K-struvite, magnesium hydroxide, calcium hydroxide, calcium carbonate, hydroxyapatite, dicalcium phosphate, and tricalcium phosphate.

2.2.3.1 Uncertainty in livestock organic waste composition

The variability in the composition of raw material creates operational difficulties that any material recovery process must deal with. The composition of cattle organic waste depends on multiple factors, among which are livestock feed, geographical area, climate, and other local factors of the livestock operation [43]. Several elements of cattle manure composition play an active role in the formation of struvite and other precipitates. These include the high ionic strength, which reduces the effective concentration of ions; and the distribution ratios between calcium, ammonia and phosphate; and the leachate alkalinity, affecting the chemical equilibrium. To capture the uncertainty generated by the variability in the composition of cattle leachate, 37 data sets of 20 literature references containing the mass fraction of different elements comprising organic livestock waste are evaluated. To estimate feasible cattle leachate compositions, the probability density distribution of each element is calculated by fitting it to the kernel density estimate (KDEs). The selected probability density distributions are normal distribution, as shown in Eq. 2.3, for the distribution of nitrogen, nitrogen as ammonia/total nitrogen ratio, and phosphorus; and lognormal distribution, as defined by Eq. 2.4, for phosphorus as phosphate/total phosphorus ratio, calcium, and potassium. The probability density distribution parameters for each evaluated compound are collected in Table 2.1, where σ is the standard deviation, σ^2 is the variance, μ is the mean of the distribution, M is equal to e^μ , and γ is a displacement parameter. Kernel density estimations and probability density distributions for each element evaluated can be found in the Supplementary Material.

The uncertainty in the composition of cattle waste is addressed through the evaluation of the thermodynamic model described in the following sections for multiple cattle waste compositions generated including the probability density distribution of each elements in a Monte Carlo model [45].

$$f(x) = \frac{1}{\sqrt{2\pi}\sigma} e^{-\frac{(x-\mu)^2}{2\sigma^2}} \quad (2.3)$$

$$f(x) = \frac{\frac{1}{x-\gamma}\sigma\sqrt{2\pi}}{M} e^{-\frac{\ln(\frac{x-\gamma}{M})^2}{2\sigma^2}} \quad (2.4)$$

Table 2.1: Probability density distributions parameters for cattle organic waste elements.

Param.	Normal distribution		Param.	Lognormal distribution			
	N	N-NH ₄ ⁺ : N _{total}		P	P-PO ₄ ³⁻ : P _{total}	Ca	K
μ	0.3841	0.6200	0.04000	M	42.15	0.08000	0.2600
σ	0.1309	0.1250	0.03684	σ	0.0040	0.4500	0.8000
				γ	-41.53	0.04044	0.03389

2.2.3.2 Initial conditions

A set of initial conditions must be defined to establish the physico-chemical characteristics of the livestock organic material [43], see Table 2.2. Please note that pH refers the adjusted pH for optimal struvite precipitation [43, 53].

Table 2.2: Initial conditions of the livestock organic material system

Variable	Value	Unit
Temperature	298	K
pH	9	-
Electrical conductivity (EC)	18,800	μS cm
Alkalinity	3000-14500	mg of CaCO ₃
[Ca ²⁺]	0.075-0.175 (determined by Monte Carlo model)	% wt wet
[K ⁺]	0.10-0.65 (determined by Monte Carlo model)	% wt wet
[P-PO ₄ ³⁻]	0.001-0.024 (determined by Monte Carlo model)	% wt wet
[N-NH ₄ ⁺]	0.015-0.64 (determined by Monte Carlo model)	% wt wet
[Mg ²⁺]	0-10	Mg ²⁺ /PO ₄ ³⁻ molar ratio

2.2.3.3 Activities

Since the cattle waste is a highly non-ideal media due to the high concentrations of dissolved ions, activities instead of molar concentrations are used in the model. Activity coefficients (γ_x) for a element x are calculated using the Debye-Hückel relationship, Eq. 2.6, which relates activity coefficient, temperature, and ionic strength, calculated using Eq. 2.5. Eq. 2.7 is employed to estimate the parameter A [24, 43]. Finally, activities for each compound are calculated using Eq. 2.8

$$I = 1.6 \cdot 10^{-5} \cdot EC, \quad I(M), \quad EC \left(\frac{\mu S}{cm} \right) \quad (2.5)$$

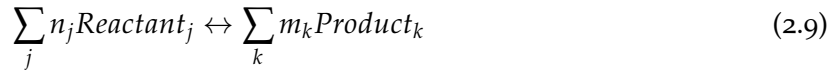
$$\log_{10}(\gamma_x) = -A \cdot z_x^2 \cdot \left(\frac{\sqrt{I}}{1 + \sqrt{I}} \right) - 0.3 \cdot I \quad (2.6)$$

$$A = 0.486 - 6.07 \cdot 10^{-4} \cdot T + 6.43 \cdot 10^{-6} \cdot T^2, \quad T(K) \quad (2.7)$$

$$\{x\} = [x] \cdot \gamma_x \quad (2.8)$$

2.2.3.4 Distribution of species in aqueous phase

The distribution of species for ammonia, water, phosphoric acid, and carbonate systems in cattle leachate is determined by chemical equilibria:



where n_j and m_k are the stoichiometric coefficients of the reactants and products respectively, and defining J as the set of chemical systems described in Table 2.3 for water, ammonia, and phosphoric acid systems, the thermodynamic equilibrium is defined for all the elements of the set as shown in Eq. 2.10. In combination with the material balances, Eq. 2.11, these define the chemical equilibrium for all the elements of the set. The description of the model for carbonate system is detailed in the Supplementary Material, and pK values are collected in Table 2.3.

$$K_J = \frac{(\prod_k \{Products\}_k^{m_k})_J}{(\prod_j \{Reactants\}_j^{n_j})_J} \quad (2.10)$$

$$[i]_J^{initial} = \sum_J [Compounds]_J \quad (2.11)$$

$$i \in \{\text{NH}_4^+, \text{Ca}^{2+}, \text{Mg}^{2+}, \text{PO}_4^{3-}, \text{CO}_3^{2-}\}$$

2.2.3.5 Precipitates formation

The precipitates that can be potentially formed from cattle waste have been selected based on the precipitates reported by previous studies [13, 15, 43]. A general solubility equilibrium, where n_a and m_b are the stoichiometric coefficients of the reactants and solid products respectively, can be written as:



Table 2.3: pK_{sp} values for the considered aqueous phase chemical systems.

Name	Chemical system	pK	Source
Ammonia	$\text{NH}_4^+ \leftrightarrow \text{NH}_3 + \text{H}^+$	9.2	[3]
Water	$\text{H}_2\text{O} \leftrightarrow \text{OH}^- + \text{H}^+$	14	[41]
	$\text{H}_3\text{PO}_4 \leftrightarrow \text{H}_2\text{PO}_4^- + \text{H}^+$	2.1	[29]
Phosphoric acid	$\text{H}_2\text{PO}_4^- \leftrightarrow \text{HPO}_4^{2-} + \text{H}^+$	7.2	[29]
	$\text{HPO}_4^{2-} \leftrightarrow \text{PO}_4^{3-} + \text{H}^+$	12.35	[29]
Carbonic acid	$\text{H}_2\text{CO}_3 \leftrightarrow \text{HCO}_3^- + \text{H}^+$	6.35	[41]
	$\text{HCO}_3^- \leftrightarrow \text{CO}_3^{2-} + \text{H}^+$	10.33	[41]

Table 2.4: Solids species considered in this work.

Name	Chemical system	pK_{sp}	Source
Struvite	$\text{MgNH}_4\text{PO}_4 \cdot 6\text{H}_2\text{O} \leftrightarrow \text{Mg}^{2+} + \text{NH}_4^+ + \text{PO}_4^{3-}$	13.26	[29]
K-struvite	$\text{MgKPO}_4 \cdot 6\text{H}_2\text{O} \leftrightarrow \text{Mg}^{2+} + \text{K}^+ + \text{PO}_4^{3-}$	10.6	[44]
Hydroxyapatite	$\text{Ca}_5(\text{PO}_4)_3\text{OH} \leftrightarrow 5\text{Ca}^{2+} + 3\text{PO}_4^{3-} + \text{OH}^-$	44.33	[7]
Calcium carbonate	$\text{CaCO}_3 \leftrightarrow \text{Ca}^{2+} + \text{CO}_3^{2-}$	8.48	[25]
Tricalcium phosphate	$\text{Ca}_3(\text{PO}_4)_2 \leftrightarrow 3\text{Ca}^{2+} + 2\text{PO}_4^{3-}$	25.50	[12]
Dicalcium phosphate	$\text{CaHPO}_4 \leftrightarrow \text{Ca}^{2+} + \text{HPO}_4^{2-}$	6.57	[14]
Calcium hydroxide	$\text{Ca}(\text{OH})_2 \leftrightarrow \text{Ca}^{2+} + 2\text{OH}^-$	5.19	[41]
Magnesium hydroxide	$\text{Mg}(\text{OH})_2 \leftrightarrow \text{Mg}^{2+} + 2\text{OH}^-$	11.15	[41]

The solid species considered in this study and their corresponding pK_{sp} values are shown in Table 2.4. These are the main precipitates that can be formed from the ions found in the cattle leachate. Considering the activity of solid species is equal to 1, and defining L as the set of chemical systems described in Table 2.4, the solubility equilibrium is defined for all the elements of the set as shown in Eq. 2.13.

The supersaturation index (Ω) is defined as the ratio between the ion activity product and the solubility product (K_{sp}), as shown in Eq. 2.14 [43]. Therefore, the value of Ω determines if a compound precipitates. A saturation index $\Omega > 1$ indicates supersaturated conditions where precipitate may form, $\Omega = 1$ indicates equilibrium between solid and liquid phases, and $\Omega < 1$ indicates unsaturated conditions where no precipitate can form.

The higher value of the supersaturation index, the larger formation potential of a precipitate. Therefore, the sequence for the precipitation

of different species can be set by comparing the supersaturation index values. The amount of solid species generated is computed through material balances, Eq. 2.15.

$$K_{sp_L} = \left(\prod_a \{Reactants\}_a^{n_a} \right)_L \quad (2.13)$$

$$\Omega_L = \frac{\left(\prod_a \{Reactants\}_a^{n_a} \right)_L}{K_{sp_L}} \quad (2.14)$$

$$[i]_L^{initial} = \sum_L [Compounds]_L \quad (2.15)$$

$$i \in \{\text{NH}_4^+, \text{Ca}^{2+}, \text{Mg}^{2+}, \text{PO}_4^{3-}, \text{CO}_3^{2-}\}$$

2.2.3.6 Thermodynamic model algorithm

Figure 2.1 shows a flowchart describing the proposed algorithm to solve the thermodynamic model of solid compound formation in cattle organic waste. In step *a*, the operating conditions and the initial molar concentrations of Ca^{2+} , K^+ , Mg^{2+} , NH_4^+ , and PO_4^{3-} in cattle leachate are defined as described previously. In step *b*, ionic strength and activity coefficients are computed. Next, in steps *c* and *d*, two parallel problems are solved, the equilibrium of the aqueous species, and the alkalinity problem to determine the distribution of carbonates. After determining the concentration of all species in the organic waste, the supersaturation index for all species is computed in step *e*. The compound with the maximum supersaturation index is assumed to precipitate first. The amount of formed precipitate is computed by solving the solubility equilibrium and the material balance. As a result of the precipitate formation, the concentration of some species in aqueous phase is reduced. Therefore, the equilibrium of the aqueous species and the alkalinity problem must be recalculated, to obtain the new concentration values of the different compounds in the waste, and the iterative process, starts again.

The iterative process runs until each component saturation index is equal or less than one, and the formation of the precipitates stops.

2.2.3.7 Integration of waste composition uncertainty and precipitates formation thermodynamic models

The evaluation of livestock waste variability in the formation of struvite and other precipitates, consists of 5 steps, as shown in Fig. 2.2. First, cattle waste composition data are collected from literature. Using these data, probability density distributions for the compounds of cattle leachate are estimated, and they are used in the Monte Carlo model to obtain feasible composition data sets of cattle organic waste. Random points are generated for each chemical compound and species ratios (i.e. N, P, K, Ca, $\text{N-NH}_4^+ : \text{N}_{total}$, and $\text{P-PO}_4^{3-} : \text{P}_{total}$). Finally,

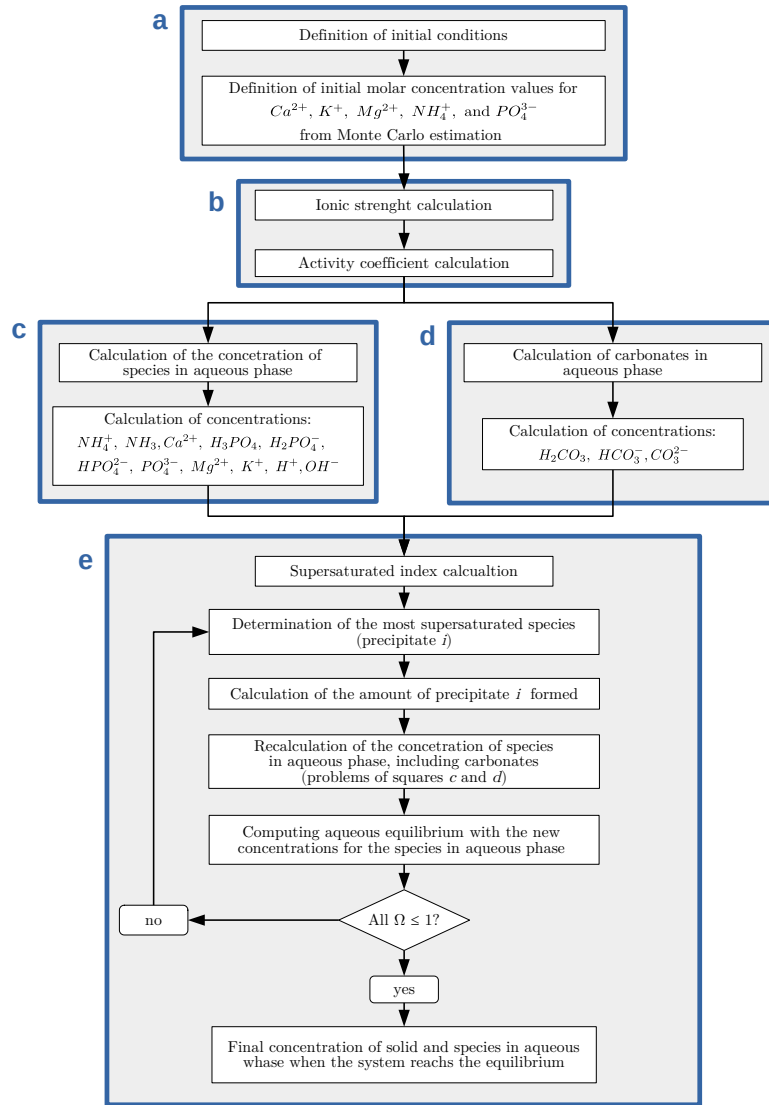


Figure 2.1: Flowchart of the proposed algorithm to solve the thermodynamic model for the formation of precipitates in cattle organic waste.

the thermodynamic model is solved for the composition data sets generated, obtaining the precipitated compounds formed.

The thermodynamic model has been implemented in the algebraic modeling language JuMP, embedded in the programming language Julia [6, 10]. The statistical study of cattle waste composition data, the Monte Carlo framework, result analysis, and data visualization were made in Python language [17, 18, 34, 51].

2.2.3.8 Model validation and limitations

The developed model was validated using the data provided by Zeng and Li [53]. Their work was carried out under similar operational conditions to which this work intends to evaluate. In Fig. 2.3

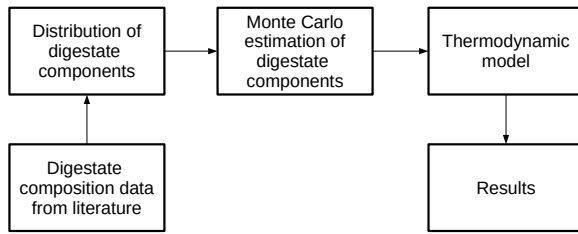


Figure 2.2: A solution procedure to evaluate the influence of the cattle waste composition variability in the formation of struvite.

experimental and model results are compared. The values at high Mg^{2+} molar ratio, when the largest supersaturation values are reached and the formation of struvite is close to the maximum allowed by the thermodynamic equilibrium, match the experimental data. However, at lower ratios, differences between results of the thermodynamic model proposed and experimental data can be observed. As the authors of the article indicate, this differences can be due to the presence of many suspended solids which interfere in the struvite formation process. Note that this work is focused on the thermodynamic aspect, without considering other aspects such as chemical kinetics or transport phenomena. The scarcity of data is an impediment to further validate the model.

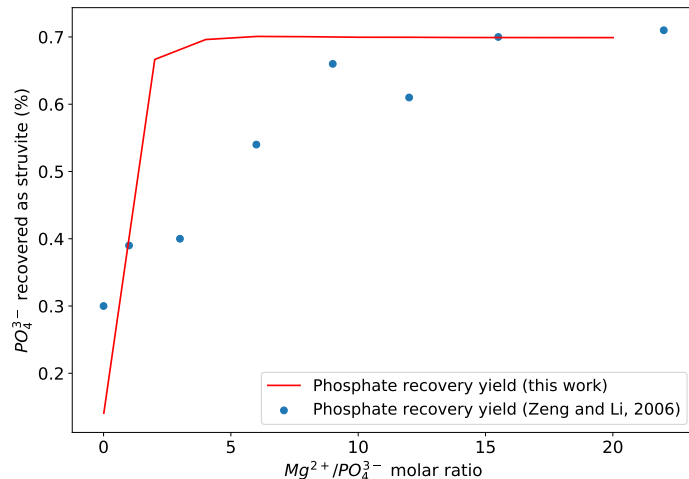


Figure 2.3: Comparison between experimental results reported by Zeng and Li [53] and the results provided by the model developed in this work.

In addition to the lack of previous studies and data availability to evaluate the effects of kinetics and transport phenomena in the formation precipitates from cattle leachate, another improvement of the proposed model can be achieved by the experimental determination of pK_{sp} values for the potential precipitates formed from cattle leachate. For struvite, the selected pK_{sp} value is taken from the work

of Ohlinger, Young, and Schroeder [29], as they determined the pK_{sp} value for struvite formation in digestate, a medium with high organic load and dissolved elements like cattle leachate. Otherwise, when pK_{sp} data for cattle waste is unavailable from previous studies, the reported values for water are used. A limitation in the use of the obtained surrogate models is that the formation of struvite and calcium precipitates can only be determined for cattle waste. Although a general formulation for the thermodynamic model is used, and the methodology proposed to include the effect of the uncertainty is not restricted to the use of a specific waste, only cattle leachate has been considered in this study. However, if data on the composition is available, surrogate models to predict the formation of struvite and calcium precipitates from other waste sources can be easily developed.

2.3 RESULTS AND DISCUSSION

2.3.1 Surrogate models to estimate the formation of precipitates from livestock organic waste

The influence of the main controllable parameters for struvite production at industrial scale operation was evaluated: the presence of magnesium and calcium, and the alkalinity. Surrogate models were developed to allow the analytical estimation of precipitates formation. pH value for the struvite precipitation process has been considered as a fixed variable, since there is a wide consensus about a pH value of 9, at which struvite solubility is minimum, is optimal, enhancing the phosphorus and nitrogen conversion to struvite and its eventual precipitation [43, 53].

2.3.1.1 Influence of magnesium

In phosphorus recovery processes through struvite formation, magnesium is usually added to increase the saturation of struvite, enhancing its precipitation. This is especially important for cattle leachate due to the high presence of calcium ions competing with other cations for phosphate anions, and the high ionic strength of livestock leachate, reducing the effective concentration of ions. If the supplementation of magnesium provides enough magnesium ions, struvite will reach higher supersaturation ratio than calcium precipitates, leading the formation of struvite over calcium compounds. To estimate the performance of struvite precipitation from cattle leachate, the developed thermodynamic model was solved for 50 different composition data sets. The average alkalinity value of the range reported by Tao, Fattah, and Huchzermeier [43] is considered, 8770.5 mg of CaCO₃. The plots showing evolution of precipitates formation in function of the Mg²⁺ / PO₄³⁻ molar ratio are collected in the Supplementary Material. Analyzing the average fraction of PO₄ recovered in form of struvite

as a function of the Mg^{2+}/PO_4^{3-} molar ratio, a tentative value for Mg^{2+}/PO_4^{3-} molar ratio between 2 and 4 can be set as a compromise effectiveness-cost solution. Higher values result in a considerable consumption of magnesium returning lower improvements in phosphate recovery as struvite. The surrogate model obtained to evaluate performance of struvite precipitation in function of the magnesium supplied is a Monod type equation, as shown in Eq. 2.16, where $x_{Mg^{2+}:PO_4^{3-}}$ is referred to the Mg^{2+}/PO_4^{3-} molar ratio.

$$x_{\text{struvite}}(PO_4^{3-}) = \frac{0.957 \cdot x_{Mg^{2+}:PO_4^{3-}}}{0.996 + x_{Mg^{2+}:PO_4^{3-}}} \quad (2.16)$$

The evolution in the formation of calcium precipitates as a function of the Mg^{2+}/PO_4^{3-} molar ratio was also studied. Hydroxyapatite and calcium carbonate are the only calcium precipitates produced. Both hydroxyapatite and $CaCO_3$ patterns can be related to the increment of struvite formation along the increase of Mg^{2+}/PO_4^{3-} molar ratio values, which reduces the presence of phosphate ions, and consequently decreases the supersaturation of hydroxyapatite. Therefore, there are more calcium ions available to form calcium carbonate. Surrogate models fit to first order polynomial equations for hydroxyapatite, Eq. 2.18, and for calcium carbonate, Eq. 2.17.

$$x_{\text{hydroxyapatite}}(Ca^{2+}) = -1.299 \cdot 10^{-2} \cdot x_{Mg:PO_4^{3-}} + 0.248 \quad (2.17)$$

$$x_{CaCO_3}(Ca^{2+}) = 1.296 \cdot 10^{-2} \cdot x_{Mg:PO_4^{3-}} + 0.749 \quad (2.18)$$

2.3.1.2 Influence of calcium

One of the hindrances of cattle leachate for struvite precipitation is the presence of calcium ions competing with other cations for phosphate to form different precipitates. To study the inhibitory influence of calcium in cattle leachate for struvite precipitation, the thermodynamic model was evaluated for the same 50 different composition data sets used in the previous study along Ca^{2+}/PO_4^{3-} molar ratio values from 0 to 5. To exclude the influence of magnesium concentration, the study was carried out fixing the Mg^{2+}/PO_4^{3-} molar ratio at 2. The plots showing evolution of precipitates formation in function of the Ca^{2+}/PO_4^{3-} molar ratio are collected in the Supplementary Material.

The phosphorus as phosphate fraction recovered as struvite exhibits a steep descent at Ca^{2+}/PO_4^{3-} values between 0 and 2, followed by an asymptotic behavior tending to 0. The dispersion of the values has slight variations along with the evaluated Mg^{2+}/PO_4^{3-} values. For hydroxyapatite and calcium carbonate, the higher Ca^{2+}/PO_4^{3-} value, the greater dispersion for the obtained values. This is due to the increase in the supersaturation values for both calcium precipitates

because of the presence of a higher number of calcium ions in the leachate.

The surrogate models obtained for struvite and calcium carbonate fit pseudo-sigmoidal equations, Eqs. 2.19 and 2.21 respectively; while for hydroxyapatite (HAP) is a second polynomial function, Eq. 2.20. In all cases, $x_{\text{Ca}^{2+}:\text{PO}_4^{3-}}$ is referred to $\text{Ca}^{2+}/\text{PO}_4^{3-}$ molar ratio.

$$x_{\text{struvite}}(\text{PO}_4^{3-}) = \frac{0.798}{1 + (x_{\text{Ca}^{2+}:\text{PO}_4^{3-}} \cdot 0.576)^{2.113}} \quad (2.19)$$

$$\begin{aligned} x_{\text{hydroxyapatite}}(\text{Ca}^{2+}) = & -4.321 \cdot 10^{-2} \cdot x_{\text{Ca}^{2+}:\text{PO}_4^{3-}}^2 + 0.313 \cdot x_{\text{Ca}^{2+}:\text{PO}_4^{3-}} \\ & - 3.619 \cdot 10^{-2} \end{aligned} \quad (2.20)$$

$$x_{\text{CaCO}_3}(\text{Ca}^{2+}) = \frac{1.020}{1 + (x_{\text{Ca}^{2+}:\text{PO}_4^{3-}} \cdot 0.410)^{1.029}} \quad (2.21)$$

2.3.1.3 Influence of alkalinity

Alkalinity is a parameter which can be used to control the production of calcium precipitates. When the presence of carbonates is low, the competition between hydroxyapatite and calcium carbonate tends to benefit the first compound because the limited availability of carbonate ions reduces the supersaturation of calcium carbonate. However, the predominance of hydroxyapatite reduces the formation of struvite since both elements compete for phosphate ions. Therefore, the presence of significant amounts of carbonates (performing at alkaline conditions) reduces the formation of hydroxyapatite and promotes the formation of struvite.

The results for the formation of struvite, hydroxyapatite and calcium carbonate considering the same 50 different composition data sets used in the previous studies in function of the alkalinity are collected in the Supplementary Material. It can be observed that the behavior of struvite formation and calcium carbonate are related, with an abrupt change for both elements at alkalinity values between 3,000 and 4,000 mg of CaCO_3 , reaching plateaus beyond these values. The dispersion of values follow a similar pattern for both struvite and calcium carbonate, being lower at low alkalinity values, and progressively growing until reaching a value of 4,000 mg of CaCO_3 . Beyond this value, the dispersion of values remains constant. Hydroxyapatite formation decrease continuously along the alkalinity values, being complementary with the formation of calcium carbonate.

Therefore, struvite formation from livestock leachate can be enhanced inhibiting hydroxyapatite formation by controlling the alkalin-

ity level, increasing the formation of calcium carbonate and reducing the concentration of calcium ions competing for phosphate. Pseudo-sigmoidal fits are shown in Eq. 2.22 for $x_{\text{struvite}}(\text{PO}_4^{3-})$, Eq. 2.23 for the case of hydroxyapatite, and Eq. 2.24 for calcium carbonate, where x_{Alk} is referred to alkalinity (mg |CaCO₃).

$$x_{\text{struvite}}(\text{PO}_4^{3-}) = \frac{0.695}{1 + (x_{\text{Alk}} \cdot 4.229 \cdot 10^{-4})^{-2.638}} \quad (2.22)$$

$$x_{\text{hydroxyapatite}}(\text{Ca}^{2+}) = \frac{0.260}{1 + (x_{\text{Alk}} \cdot 6.460 \cdot 10^{-5})^{3.390}} \quad (2.23)$$

$$x_{\text{CaCO}_3}(\text{Ca}^{2+}) = \frac{0.847}{1 + (x_{\text{Alk}} \cdot 4.646 \cdot 10^{-4})^{-1.870}} \quad (2.24)$$

2.3.1.4 Interactions between calcium and magnesium to phosphate ratios

Interactions between calcium and magnesium to phosphate ratios were evaluated to determine a target operational area for optimal struvite production performance. In Fig. 2.4 the formation of struvite as function of Mg²⁺/PO₄³⁻ and Ca²⁺/PO₄³⁻ molar ratios is shown, where the area with the highest phosphate recovery in form of struvite has been shaded. It can be observed that struvite formation depends strongly on the Ca²⁺/PO₄³⁻ molar ratio. For Ca²⁺/PO₄³⁻ values less than 3 struvite formation reaches the maximum values, even for low Mg²⁺/PO₄³⁻ molar ratio values. For high calcium/phosphate ratios, struvite formation decreases abruptly, obtaining low increases in struvite formation even for large supplies of magnesium.

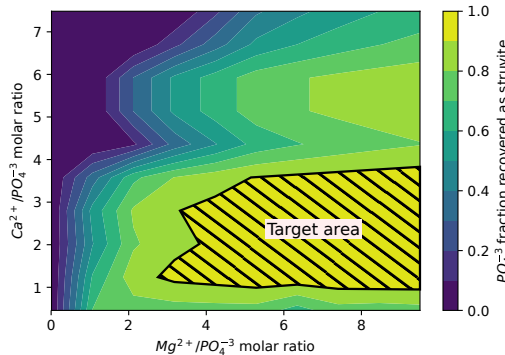


Figure 2.4: Influence of magnesium and calcium in struvite precipitation.

2.3.2 Phosphorus releases from cattle leachate potentially avoided via struvite formation

Phosphorus pollution of waterbodies, followed by eutrophication and hypoxia scenarios, represents a major environmental problem for the current societies. Considering the United States, the Census of Agriculture reports more than 93 million of cattle heads [49], generating an estimated amount of 1,144 million of tons of organic waste per year. The phosphorus contained in the organic waste can be lost as runoff, reaching waterbodies, and polluting the surrounding aquatic ecosystems. Actually, several outstanding cases of eutrophication have taken place in the U.S. in recent times, such as the events occurred in Lake Erie since 1990, and the dead zone in the Gulf of Mexico because of in-excess nutrients discharges collected along the Mississippi River basin. Therefore, nutrient recovery strategies must be implemented to capture phosphorus (and nitrogen) before reaching the waterbodies. Additionally, phosphorus recovery as struvite allows its redistribution to nutrient deficient areas [22]. The surrogate models developed are used to estimate the potential phosphorus emissions avoided in each watershed through phosphorus recovery from cattle leachate as struvite.

2.3.2.1 Balance of phosphorus involved in agricultural activities throughout the U.S. watersheds

To reach environmental sustainability and reduce the impact over the original ecosystems as much as possible, the releases of phosphorus should be balanced with a coordinated network of phosphorus uptakes. To determine the balance between the releases and uptakes of phosphorus from the agricultural sector, the TES sustainability metric is computed for each watershed in the U.S., showing the watersheds where the phosphorus releases are unbalanced and impacting the environment, Fig. 2.5. For a total of 2,104 HUC8 watersheds, data is unavailable for 6 watersheds, the phosphorus releases and uptakes are balanced in 1,410 watersheds, and 691 exhibit unbalanced phosphorus releases, representing the 33.12% of total watersheds. It can be observed a larger concentration of unbalanced watersheds along the Mississippi River basin and around the Lake Erie, areas currently affected by eutrophication issues.

For studies requiring higher spatial resolution, more accurate values for the TES metric can be stimated through the use of local inventories for phosphorus releases and uptakes. A dataset with the phosphorus releases and uptakes, the phosphorus balance, and the TES metric computed for each watershed are available in the Supplementary Material. A dataset with the phosphorus releases and uptakes, the phosphorus balance, and the TES metric computed for each watershed are available in the Supplementary Material.

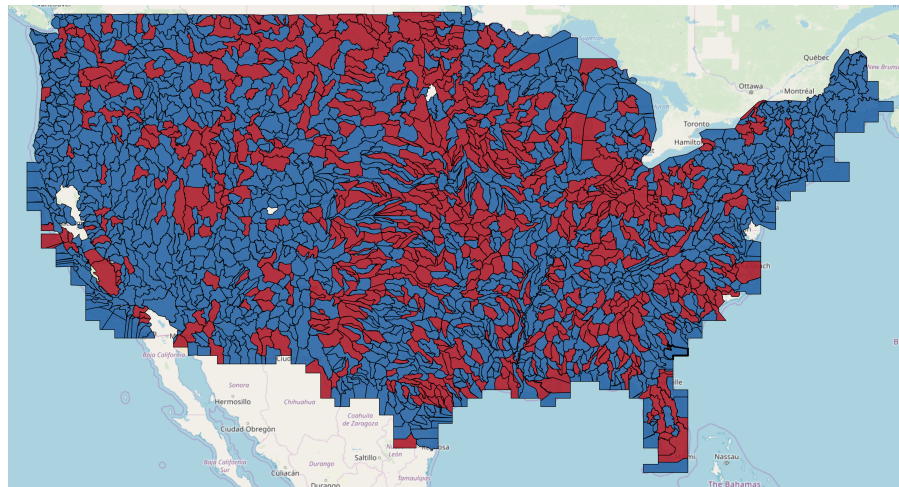


Figure 2.5: Techno-ecological synergy (TES) metric values for HUC8 watersheds. Red indicates watersheds with unbalanced agricultural phosphorus releases, and blue indicates watersheds with balanced agricultural phosphorus releases. White indicates watersheds with not available data.

2.3.2.2 *Phosphorus recovered from cattle leachate through struvite precipitation*

Since the scope of the surrogate models developed is limited to the treatment of cattle leachate, only P releases from cattle organic waste will be considered for recovery. Additionally, as it is mentioned in the description of the model, only the phosphate fraction of phosphorus can be recovered through struvite precipitation. Data provided by IPNI NuGIS [19] report total manure generated, but do not report the breakdown of manure generated by different livestock sources. Therefore, the inventory of cattle for each HUC6 watershed reported by the U.S. Census of Agriculture is used [49]. To keep spatial consistency between data, the inventory of cattle was aggregated from HUC6 to HUC8 watershed level scaling by the fraction of area represented by each HUC8 basin over the total HUC6 area. The breakdown of cattle types in the U.S. Census of Agriculture is not available at watershed level, but it is available at state level. Therefore, the number of cattle heads is weighted by the fraction of milk and beef animals in the corresponding state. Finally, the animals number for each type of cattle is calculated using the normalization values provided by Kellogg et al. (2010) [47]. If the watershed is shared among several states, the average of the represented states is considered.

Since the supply of magnesium is the easiest controllable variable in the struvite precipitation process, the scenarios evaluated to determine the phosphorus emissions avoided through struvite precipitation were defined through the use of different amounts of magnesium using the surrogate model shown in Eq. 2.16. The different supplies of

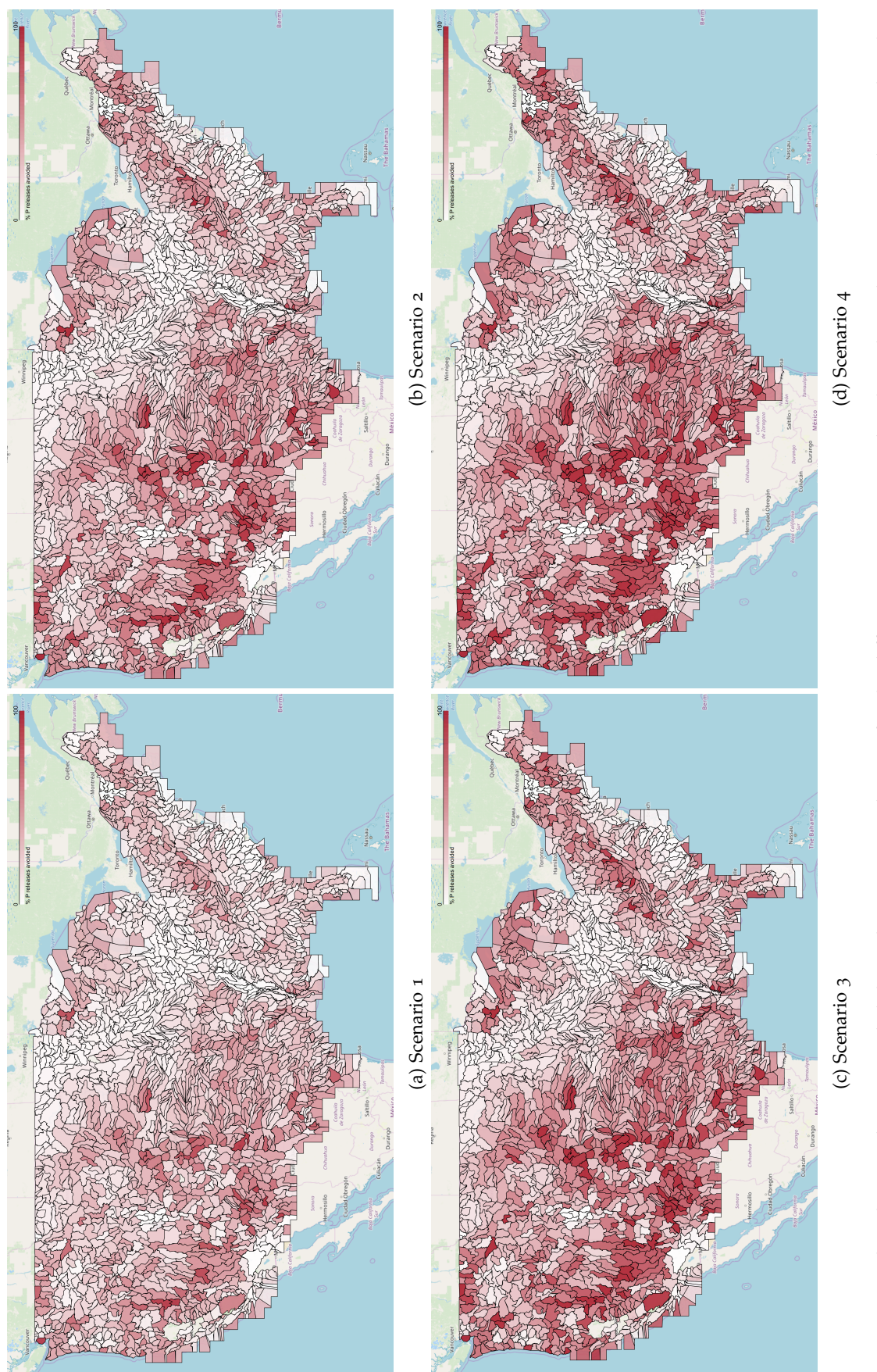


Figure 2.6: Phosphorus releases avoided through struvite production for the different scenarios considered. Darker colors represent larger phosphorus recovery

magnesium have a direct influence on the economy of the process, being one of the highest operating costs items. A summary of the scenarios evaluated and the results obtained is presented in Table 2.5. The fraction of phosphorus releases avoided is computed over the total phosphorus releases from agricultural activities, including manure releases and fertilizer application, as described in Section 2.2.2.1.

Table 2.5: Scenarios considered and results for cattle leachate phosphorus recovery

Scenario	1	2	3	4
Mg ²⁺ /PO ₄ ³⁻ molar ratio	1	2	4	6
Total P releases avoided (total watersheds) (tons)	422,104	562,430	674,556	722,573
Average P releases avoided (total watersheds) (%)	22.63	30.16	36.17	38.75
Average P releases avoided (unbalanced watersheds) (%)	18.07	24.08	28.88	30.94
kg Mg/kg P recovered	2.68	4.02	6.71	9.40

The results for each scenario considered at watershed scale are shown in Fig. 2.6, where darker colors represent larger phosphorus releases avoided. It can be observed that struvite production can contribute to reducing phosphorus emissions around Lake Erie and the Great Lakes region, one of the most severely affected areas by eutrophication problems. Additionally, other areas where the phosphorus emissions avoided are especially significant are the upper basin of the Mississippi River, and the basins located in the south-central region of the United States, such as the areas of some tributaries rivers to the Mississippi River basin, the Rio Grande river and the Colorado River basin. At national level, struvite production can contribute to reduce the agricultural phosphorus releases by 22% for most conservative case where the lowest amount of magnesium is added. The phosphorus fraction recovered raises until a 30% and 36% when the amount of magnesium added is multiplied by 2 and by 4 respectively. However, for the scenario 4 the increase in the supply of magnesium only increases the phosphorus recovered in 2 percentual points compared with the previous scenario. Therefore, the implementation of struvite production processes for phosphorus recovering in cattle facilities can contribute significantly to the reduction in the phosphorus emissions from agricultural operations, reducing the runoffs to waterbodies and mitigating the nutrient pollution of the aquatic ecosystems. However, when only unbalance watersheds are considered, the average fraction of phosphorus releases avoided decreases, suggesting that, from a

global overview, the phosphorus releases due to fertilizers play a major role in these watersheds than when balance and unbalance watersheds are evaluated altogether. Data at watershed level are collected in the Supplementary Material.

Therefore, the phosphorus recovered from livestock facilities have a significant impact in the reduction of phosphorus releases to the environment. However, to achieve a successful implementation of nutrient management strategies, coordinated network management efforts to mitigate nutrient pollution of aquatic systems including point and non-point sources, should be performed for optimizing nutrient management programs that minimize the capital and operating costs while maximizing the environmental benefits. Proposals for the development of coordinated management systems for organic wastes have been presented by Sharara et al. [39], Sampat et al. [36], and Hu et al. [16].

2.4 CONCLUSIONS

To estimate the potential phosphorus releases avoided through struvite precipitation from cattle waste, a thermodynamic framework has been developed to evaluate struvite production from cattle organic waste as a technology for nutrient management and recovery. A set of practical numerical correlations is developed to help predict the struvite recovery. Cattle waste treatment and nutrient recovery through struvite formation is a feasible process from a thermodynamic perspective, reaching phosphate recovery efficiencies up to 80% with the addition of considerable amounts of magnesium. Additionally, the results show that alkaline conditions can control the calcium ions when their presence in the medium is high and these can interfere in the formation of struvite by precipitating the calcium ions as calcium carbonate, and enhancing the recovery of phosphate as struvite. However, the variability in the organic waste composition is an important parameter that has a high impact on the efficiency of the process. Therefore, an individual composition analysis of the treated cattle waste should be the ideal procedure to achieve the optimal performance of the process by adjusting the operating conditions, particularly the amount of magnesium added and the alkalinity of the medium. Nevertheless, there are opportunities for improving the proposed model by the experimental determination of pK_{sp} values for all potential precipitates from cattle leachate, and by including the effects from kinetics and transport phenomena.

The techno-ecological synergy sustainability metric (TES) is a useful tool for visualizing the spatial distribution of environmental problems, making it possible to determine what areas are more sensible to nutrient pollution, and allowing an adequate distribution of efforts to mitigate phosphorus releases and achieved better nutrient manage-

ment practices. In the U.S., struvite production has large potential for reducing the phosphorus losses from livestock facilities, avoiding between the 22% and the 36% of the phosphorus releases from the agricultural sector at national level, reducing the phosphorus runoff and mitigating the nutrient pollution of waterbodies. In addition, it can be observed how struvite production can significantly contribute to reducing phosphorus emissions around Lake Erie and the Great Lakes region, some of the most severely affected areas by eutrophication problems. It should be remarked that the production of struvite from cattle leachate allows the redistribution of phosphorus to nutrient deficient areas reducing the phosphorus runoff to waterbodies and mitigating the nutrient pollution of aquatic ecosystems. However, future research is needed to consider temporal aspects, transportation logistics, and coordinated management strategies for achieving global solutions to global problems.

NOMENCLATURE

Variables

A	parameter of the Debye-Hückel relationship
EC	electrical conductivity ($\frac{\mu S}{cm}$)
E_x	emissions of component x
I	ionic strength (M)
K	thermodynamic equilibrium constant
K_{sp}	solubility product
M	equal to e^μ
T	temperature (K)
U_x	uptakes of component x
V_x	techno-ecological synergy sustainability metric for component x
Ω	supersaturation ratio
γ	displacement parameter
γ_x	activity coefficient for a element x
μ	mean of the distribution
σ	standard deviation
σ^2	variance
m	stoichiometric coefficient
n	stoichiometric coefficient
x_{Alk}	alkalinity (mg $CaCO_3$)
x_{CaCO_3}	fraction of calcium recovered as calcium carbonate
$x_{Ca^{2+}:PO_4^{3-}}$	Ca^{2+}/PO_4^{3-} molar ratio

$x_{Mg^{2+};PO_4^{3-}}$	Mg^{2+}/PO_4^{3-} molar ratio
$x_{hydroxyapatite(Ca^{2+})}$	fraction of calcium recovered as hydroxyapatite
$x_{struvite}(PO_4^{3-})$	fraction of phosphorus as phosphate recovered as struvite
z_x	integer charge of ion x

Abbreviations

AAPFCO	Association of American Plant Food Control Officials
CAFO	Concentrated Animal Feeding Operation
HAB	Harmful Algal Bloom
HUC	Hydrologic Unit Code
KDE	Kernel Density Estimation
USDA	United States Department of Agriculture

ACKNOWLEDGMENTS

We acknowledge funding from the Junta de Castilla y León, Spain, under grant SAo26G18 and grant EDU/556/2019, and by an appointment for E. Martín-Hernández to the Research Participation Program for the Office of Research and Development, U.S. EPA, administered by the Oak Ridge Institute for Science and Education.

Disclaimer: The views expressed in this article are those of the authors and do not necessarily reflect the views or policies of the U.S. EPA. Mention of trade names, products, or services does not convey, and should not be interpreted as conveying, official U.S. EPA approval, endorsement, or recommendation.

BIBLIOGRAPHY

- [1] Richard B. Alexander, Richard A. Smith, Gregory E. Schwarz, Elizabeth W. Boyer, Jacqueline V. Nolan, and John W. Brakebill. «Differences in Phosphorus and Nitrogen Delivery to The Gulf of Mexico from the Mississippi River Basin.» In: *Environmental Science & Technology* 42.3 (2008), pp. 822–830. doi: [10.1021/es0716103](https://doi.org/10.1021/es0716103).
- [2] B.R. Bakshi, G. Ziv, and M.D. Lepech. «Techno-ecological synergy: A framework for sustainable engineering.» In: *Environ. Sci. Technol.* 49.3 (2015), pp. 1752–1760.
- [3] R. G. Bates and G. Pinching. «Acid dissociation constant of ammonium ion at 0–50 °C, and the base strength of ammonia.» In: *Journal of Research of the National Bureau of Standards* 42 (1949), pp. 419–430.

- [4] P. Battistoni, A. De Angelis, P. Pavan, M. Prisciandaro, and F. Cecchi. «Phosphorus removal from a real anaerobic supernatant by struvite crystallization.» In: *Wat. Res.* 35 (2001), pp. 2167–2178.
- [5] J.J. Beaulieu, T. DelSontro, and J.A. Downing. «Eutrophication will increase methane emissions from lakes and impoundments during the 21st century.» In: *Nat. Commun.* 10 (2019), p. 1375.
- [6] Jeff Bezanson, Alan Edelman, Stefan Karpinski, and Viral B Shah. «Julia: A fresh approach to numerical computing.» In: *SIAM review* 59.1 (2017), pp. 65–98.
- [7] P. Brezonik and W. Arnold. *Water Chemistry An Introduction to the Chemistry of Natural and Engineered Aquatic Systems*. Oxford University Press, 2011. ISBN: 9780199730728.
- [8] Ipek Celen, John R. Buchanan, Robert T. Burns, R. Bruce Robinson, and D. Raj Raman. «Using a chemical equilibrium model to predict amendments required to precipitate phosphorus as struvite in liquid swine manure.» In: *Water Research* 41.8 (2007), pp. 1689–1696.
- [9] Dana Cordell, Jan-Olof Drangert, and Stuart White. «The story of phosphorus: Global food security and food for thought.» In: *Glob. Environ. Change.* 19.2 (2009), pp. 292–305.
- [10] Iain Dunning, Joey Huchette, and Miles Lubin. «JuMP: A Modeling Language for Mathematical Optimization.» In: *SIAM Review* 59.2 (2017), pp. 295–320. DOI: [10.1137/15M1020575](https://doi.org/10.1137/15M1020575).
- [11] D.A. Dzombak. «Nutrient Control in Large-Scale U.S. Watershed. The Chesapeake Bay and Northern Gulf of Mexico.» In: *The Bridge* 41.4 (2011), pp. 13–22.
- [12] B.O. Fowler and S. Kuroda. «Changes in heated and in laser-irradiated human tooth enamel and their probable effects on solubility.» In: *Calcif. Tissue. Int.* 38 (1986), pp. 197–208.
- [13] Sachin Gadekar and Pratap Pullammanappallil. «Validation and applications of a chemical equilibrium model for struvite precipitation.» In: *Environmental modeling & assessment* 15.3 (2010), pp. 201–209.
- [14] T.M. Gregory, E.C. Moreno, and W.E. Brown. «Solubility of $\text{CaHPO}_4 \cdot 2\text{H}_2\text{O}$ in the system $\text{Ca}(\text{OH})_2 - \text{H}_3\text{PO}_4 - \text{H}_2\text{O}$ at 5, 15, 25 and 37.5 °C.» In: *J. Res. Natl. Bur. Stand.* 74 (1970), pp. 461–475.
- [15] H. Harada, Y. Shimizu, Y. Miyagoshi, S. Matsui, T. Matsuda, and T. Nagasaka. «Predicting struvite formation for phosphorus recovery from human urine using an equilibrium model.» In: *Water Science and Technology* 54.8 (2006), pp. 247–255.

- [16] Yicheng Hu, Apoorva M. Sampat, Gerardo J. Ruiz-Mercado, and Victor M. Zavala. «Logistics Network Management of Livestock Waste for Spatiotemporal Control of Nutrient Pollution in Water Bodies.» In: *ACS Sustainable Chem. Eng.* 7.22 (2019), pp. 18359–18374. doi: [10.1021/acssuschemeng.9b03920](https://doi.org/10.1021/acssuschemeng.9b03920).
- [17] John D. Hunter. «Matplotlib: A 2D Graphics Environment.» In: *Comput Sci Eng* 9 (2007), pp. 90–95.
- [18] John D. Hunter. «Data Structures for Statistical Computing in Python.» In: *Proceedings of the 9th Python in Science Conference*, (2010), pp. 51–56.
- [19] International Plant Nutrition Institute (IPNI). *A Nutrient Use Information System (NuGIS) for the U.S.* Tech. rep. International Plant Nutrition Institute (IPNI), 2012.
- [20] R.H. Kadlec. «Large Constructed Wetlands for Phosphorus Control: A Review.» In: *Water* 8 (2016), p. 243.
- [21] D Mangin and JP Klein. «Fluid dynamic concepts for a phosphate precipitation reactor design.» In: *Phosphorus in environmental technologies: Principles and applications*. IWA Publishing London, UK, 2004, pp. 358–401.
- [22] E. Martín-Hernández, A.S. Sampat, V.M. Zavala, and M. Martín. «Optimal integrated facility for waste processing.» In: *Chem. Eng. Res. Des.* 131 (2018), pp. 160–182.
- [23] A. Matynia, B. Wierzbowska, N. Hutnik, A. Mazienczuk, A. Kozik, and K. Piotrowski. «Separation of struvite from mineral fertilizer industry wastewater.» In: *Procedia. Environ. Sci.* 18 (2013), pp. 766–775.
- [24] Metcalf and Eddy. *Wastewater Engineering: Treatment and Resource Recovery*. McGraw-Hill, New York, 2014. ISBN: 9780071122504.
- [25] John W. Morse, Rolf S. Arvidson, and Andreas Lüttege. «Calcium Carbonate Formation and Dissolution.» In: *Chem. Rev.* 107 (2007), pp. 342–381.
- [26] Atif Muhammed, Jiaxin Lu, Renjie Dong, and Shubiao Wu. «Formation of struvite from agricultural wastewaters and its reuse on farmlands: Status and hindrances to closing the nutrient loop.» In: *Journal of environmental management* 230 (2019), pp. 1–13.
- [27] Ohio State University Extension. *Ohio Agronomy Guide, 14th Edition*. Tech. rep. Ohio State University Extension, 2005.
- [28] Ohio State University Extension. *Ohio Agronomy Guide, 15th Edition*. Tech. rep. Ohio State University Extension, 2017.
- [29] K. N. Ohlinger, T.M. Young, and E.D. Schroeder. «Predicting struvite formation in digestion.» In: *Wat. Res.* 32.12 (1998), pp. 3607–3614.

- [30] B. R. Pickard, J. Daniel, M. Mehaffey, L. E. Jackson, and A. Neale. «EnviroAtlas: A new geospatial tool to foster ecosystem services science and resource management.» In: *Ecosyst. Serv.* 14 (2015), pp. 45–55.
- [31] Md Saifur Rahaman, Donald S. Mavinic, Alexandra Meikleham, and Naoko Ellis. «Modeling phosphorus removal and recovery from anaerobic digester supernatant through struvite crystallization in a fluidized bed reactor.» In: *Water Research* 51 (2014), pp. 1–10.
- [32] I. R. Richards and A. E. Johnston. *The effectiveness of different precipitated phosphates as sources of phosphorus for plants*. Tech. rep. CEEP, European Fertiliser Manufacturers Association, Anglian Water UK, Thames Water UK and Berlin Wasser Betriebe, 2001.
- [33] Mariska Ronteltap, Max Maurer, and Willi Gujer. «Struvite precipitation thermodynamics in source-separated urine.» In: *Water Research* 41.5 (2007), pp. 977–984.
- [34] G. van Rossum. *Python tutorial*. Tech. rep. CS-R9526. Amsterdam: Centrum voor Wiskunde en Informatica (CWI), May 1995.
- [35] K.C. Ruttenberg. «Phosphorus Cycle*.» In: *Encyclopedia of Ocean Sciences (Second Edition)*. Ed. by John H. Steele. Second Edition. Oxford: Academic Press, 2001, pp. 401–412. ISBN: 978-0-12-374473-9.
- [36] A.M. Sampat, Y Hu, M Sharara, H Aguirre-Villegas, G.J. Ruiz-Mercado, R.A. Larson, and V. M. Zavala. «Coordinated management of organic waste and derived products.» In: *Comput. Chem. Eng.* 128 (2019), pp. 352–363.
- [37] A.S. Sampat, E. Martín, M. Martín, and V.M. Zavala. «Optimization formulations for multi-product supply chain networks.» In: *Comput. Chem. Eng.* 104 (2017), pp. 296–310.
- [38] A.S. Sampat, G. J. Ruiz-Mercado, and V.M. Zavala. «Economic and Environmental Analysis for Advancing Sustainable Management of Livestock Waste: A Wisconsin Case Study.» In: *ACS Sustain. Chem. Eng.* 6.5 (2018), pp. 6018–6031.
- [39] Mahmoud Sharara, Apoorva Sampat, Laura W. Good, Amanda S. Smith, Pamela Porter, Victor M. Zavala, Rebecca Larson, and Troy Runge. «Spatially explicit methodology for coordinated manure management in shared watersheds.» In: *J. Environ. Manage.* 192 (2017), pp. 48–56.
- [40] Utsav Shashvatt, Josh Benoit, Hannah Aris, and Lee Blaney. «CO₂-assisted phosphorus extraction from poultry litter and selective recovery of struvite and potassium struvite.» In: *Wat. Res.* 143 (2018), pp. 19–27.

- [41] D.A. Skoog, D.M. West, F.J. Holler, and S.R Crouch. *Fundamentals of analytical chemistry*. Cengage Learning, 2014. ISBN: 9780495558286.
- [42] Richard A. Smith and Richard B. Alexander. *Sources of Nutrients in the Nation's Watersheds*. Tech. rep. U. S. Geological Survey, 1999.
- [43] W. Tao, K.P. Fattah, and M.P. Huchzermeier. «Struvite recovery from anaerobically digested dairy manure: A review of application potential and hindrances.» In: *J. Environ. Manage.* 169 (2016), pp. 46–57.
- [44] A.W. Taylor, A.W. Frazier, and E.L. Gurneynum. «Solubility products of magnesium ammonium and magnesium potassium phosphates.» In: *Trans. Faraday Soc.* 59 (1963), pp. 1580–1584.
- [45] P. Thomopoulos. *Essentials of Monte Carlo Simulation*. Springer, New York, 2012.
- [46] U.S. Geological Survey. *Federal Standards and Procedures for the National Watershaed Boundary Dataset (WBD)*. Tech. rep. U.S. Geological Survey, 2013.
- [47] United States Department of Agriculture. *Manure Nutrients Relative to the Capacity of Cropland and Pastureland to Assimilate Nutrients*. Tech. rep. United States Department of Agriculture, 2000.
- [48] United States Department of Agriculture (USDA). *Waste Management Field Handbook*. Tech. rep. 2009.
- [49] United States Department of Agriculture (USDA). *2017 Census of Agriculture. United Satates. Summary and State Data*. Tech. rep. 2019.
- [50] United States Department of Agriculture (USDA), National Agricultural Statistics Service. *Cattle (January 2020)*. Tech. rep. 2020.
- [51] S van der Walt, S.C. Colbert, and G. Varoquaux. «The NumPy Array: A Structure for Efficient Numerical Computation.» In: *Comput Sci Eng* 13 (2011), pp. 22–30.
- [52] Hanlu Yan and Kaimin Shih. «Effects of calcium and ferric ions on struvite precipitation: A new assessment based on quantitative X-ray diffraction analysis.» In: *Wat. Res.* 95 (2016), pp. 310–318.
- [53] L. Zeng and X. Li. «Nutrient removal from anaerobically digested cattle manure by struvite precipitation.» In: *J. Environ. Eng. Sci.* 5 (2006), pp. 285–294.

Part II
APPENDIX

A

APPENDIX A: SUPPLEMENTARY INFORMATION OF CHAPTER 2

All the units involved in the flowsheet are modeled using mass and energy balances, thermodynamic relationships, chemical and vapor-liquid equilibria, and product yield calculations. Therefore, the variables of the equation oriented framework comprise the total mass flows, component mass flows, component mass fractions, temperatures and pressures of the streams in the process network. The components that are tracked in our calculations belong to the following set:

{Wa, CO₂, CO, O₂, N₂, H₂S, NH₃, CH₄, SO₂, C, H, O, N, N_{org}, P, K, S, Rest, Cattle slurry, Pig slurry, Poultry slurry, P₂O₅, CaCO₃, FeCl₃, Antifoam, Fe₂(SO₄)₃, Al₂(SO₄)₃, AlCl₃, MgCl₂, NaOH, Struvite seeds, Mg, Cl, Struvite, K-Struvite, MgCl₂ CSTR, NaOH CSTR, Mg CSTR, Cl CSTR, Struvite CSTR, KStruvite CSTR, FeCl₃ Coag}

In the following subsections we briefly present the main equations used to characterize the operation of the different units. Simpler balances based on removal efficiency or stoichiometry, or the equations that connect two units are omitted and only the conversion, the chemical reactions, and the removal efficiency are presented.

The decision on the technology to use to process the digestate requires the evaluation of the cost. Its estimation uses the factorial method based on the equipment units costs Sinnott [10]. The total physical plant cost involving equipment erection, piping instrumentation, electrical, buildings, utilities, storages, site development, and ancillary buildings is 3.15 times the total equipment cost for processes which uses fluids and solids. On the other hand, the fixed cost, which includes design and engineering, contractor's fee, and contingency items is determined as 1.4 times the total physical plant cost for fluid and solid processes. In the subsequent cost estimation, these parameters are designed as f_i for the total physical plant parameter and f_j for the fixed cost parameter.

A.1 BIOGAS PRODUCTION

The anaerobic fermentation of different types of manure generates biogas, methane and carbon dioxide, through a series of reactions such as hydrolysis, acidogenesis, acetogenesis and methanogenesis

[2]. The biogas produced shows a variable composition in methane and CO₂ depending on the composition of the manure processed and the operating conditions. The lower the temperature, the longer the retention time. We operate at 55 °C for 20 days. A part from methane and CO₂, nitrogen, H₂S, and NH₃ are produced [6]. Thus, in order to compute the biogas composition a mass balance is performed considering the composition of the different manure sources:

$$MW_{dry\text{-}biogas} = \sum_{a'} Y_{a'}/biogas\text{-}dry \cdot MW_{a'} \quad (\text{A.1})$$

where the typical composition, Y_i , of the biogas is given by the following bounds:

$$\begin{aligned} 0.7 &\leq Y_{CH_4} \leq 0.5 \\ 0.3 &\leq Y_{CO_2} \leq 0.5 \\ 0.02 &\leq Y_{N_2} \leq 0.06 \\ 0.005 &\leq Y_{O_2} \leq 0.16 \\ Y_{H_2S} &\leq 0.002 \\ 9 \cdot 10^{-5} &\leq Y_{NH_3} \leq 1 \cdot 10^{-4} \end{aligned} \quad (\text{A.2})$$

The contact between biogas and the liquid residue results in biogas saturated with water. Gas moisture is computed using Antoine correlation as per Eq. A.3. The flow of dry biogas is determined using Eq A.4. To compute the power in the compressor, we need to determine the molar mass of the biogas as in Eq. A.5. The mass flow rate of each component is computed from its molecular weight and the total mass flow rate, Eqs. A.6-A.7.

$$y_{biogas} = \frac{MW_{H_2O}}{MW_{biogas\text{-}dry}} \frac{Pv(T)}{P - Pv(T)} \quad (\text{A.3})$$

$$F_{biogas} = \rho_{biogas} \sum_{Waste} w'_{SV/Waste} \cdot w_{MS/Waste} \cdot F_{Waste} \cdot V_{biogas/Waste} \quad (\text{A.4})$$

$$fc_{H_2O}^{biogas} = y_{biogas} \cdot \sum_{a'} fc_{a'}^{biogas} \quad (\text{A.5})$$

$$\begin{aligned} \frac{fc_{a'}^{Bioreactor,Compres1}}{MW_{a'}} &= \\ \frac{Y_{a'}/biogas\text{-}dry}{MW_{biogas\text{-}dry}} \left(F^{Bioreactor,Compres1} - fc_{H_2O}^{Bioreactor,Compres1} \right) \end{aligned} \quad (\text{A.6})$$

$$MW_{biogas} \sum_a \frac{x_{a/biogas}}{MW_a} = \sum_a x_{a/biogas} \quad (\text{A.7})$$

The lower and upper limits for the generation of biogas are given by Eq. A.8 [2]:

$$\begin{aligned} 0.20 &\leq V_{biogas/Waste} \leq 0.50 \\ 0.10 &\leq w_{MS/Waste} \leq 0.20 \\ 0.50 &\leq w_{VS/Waste} \leq 0.80 \end{aligned} \quad (\text{A.8})$$

The mass of waste that does not leave as biogas constitutes the digestate as follows [2]:

$$w'_{C/k} = R_{C-N/k} \left(w'_{N_{org}/k} + w'_{N_{NH_3}/k} \right) \quad (\text{A.9})$$

Each manure type has its own composition [4].

$$\begin{aligned} 6 &\leq R_{C-N/Waste} \leq 20 \\ 0.005 &\leq w_{N/Waste} \leq 0.047 \\ 0.005 &\leq w_{N_{org}/Waste} \leq 0.036 \\ 0.008 &\leq w_{P/Waste} \leq 0.013 \\ 0.033 &\leq w_{K/Waste} \leq 0.1 \end{aligned} \quad (\text{A.10})$$

$$\begin{aligned} w_{C/Waste} + w_{N_{org}/Waste} + w_{N_{NH_3}/Waste} + w_{P/Waste} + \\ w_{K/Waste} + w_{Rest/Waste} = 1 \end{aligned} \quad (\text{A.11})$$

Atom mass balances are performed to compute the products of the reactors. We consider balances for carbon, organic nitrogen (N_{org}), inorganic nitrogen (N), phosphate and potassium. The carbon either leaves in the form of CO_2 or CH_4 with the gas or as part of the waste in the digestate, Eq. A.12. The organic nitrogen in the digestate is given by the fraction of organic nitrogen in the digestate minus the nitrogen released as gas, Eq A.13. Similarly, the inorganic nitrogen that is not used to produce ammonia that accompanies the gas or is left as residue is computed using the values above, Eq. A.14. P and K directly leave the reactor as part of the digestate, Eqs. A.15-A.16. The rest that is not accounted for is assumed to be a residual part leaving the reactor with the digestate.

$$fc_C^{digestate} = w'_C \cdot w_{MS} \cdot F_{Waste} - fc_{CH_4} \frac{MW_C}{MW_{CH_4}} - fc_{CO_2} \frac{MW_C}{MW_{CO_2}} \quad (\text{A.12})$$

$$fc_{N_{org}}^{digestate} = w'_{N_{org}/Waste} \cdot w_{MS/Waste} \cdot F_{Waste} - fc_{N_2} \frac{MW_N}{MW_{N_2}} \quad (\text{A.13})$$

$$fc_N^{digestate} = w'_{N/Waste} \cdot w_{MS/Waste} \cdot F_{Waste} - fc_{NH_3} \frac{MW_N}{MW_{NH_3}} \quad (\text{A.14})$$

$$fc_P^{digestate} = w'_{P/Waste} \cdot w_{MS/Waste} \cdot F_{Waste} \quad (\text{A.15})$$

$$fc_K^{digestate} = w'_{K/Waste} \cdot w_{MS/Waste} \cdot F_{Waste} \quad (\text{A.16})$$

$$\begin{aligned} fc_{Rest}^{digestate} &= w'_{Rest/Waste} \cdot w_{MS/Waste} \cdot F_{Waste} + \\ fc_{CH_4}^{biogas} \cdot \frac{4 \cdot MW_H}{MW_{CH_4}} &- fc_{CO_2}^{biogas} \cdot \frac{2 \cdot MW_O}{MW_{CO_2}} - \\ fc_{NH_3}^{biogas} \cdot \frac{3 \cdot MW_H}{MW_{NH_3}} &- fc_{H_2S}^{biogas} - fc_{O_2}^{biogas} \end{aligned} \quad (\text{A.17})$$

$$fc_{H_2O}^{digestate} = (1 - w_{MS/Waste}) \cdot F_{Waste} - fc_{H_2O}^{biogas} \quad (\text{A.18})$$

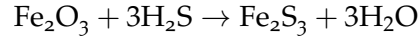
The energy balance to the digester is as follows:

$$\begin{aligned} Q_{digester} &= \Delta H_{reaction} - F \cdot c_p \cdot (T_{digester} - T_{in}) \\ \Delta H_{reaction} &= \sum_{products} \Delta H_{comb} - \sum_{reactants} \Delta H_{comb} \end{aligned} \quad (\text{A.19})$$

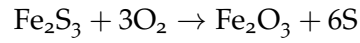
The digestate is further conditioned.

A.2 H₂S REMOVAL

Since biogas is burned for power production, any sulfur compound would potentially produce SO₂. We can avoid it by removing the H₂S. A reactive bed of Fe₂O₃ that operates at 25–50 °C is used. The actual removal is carried out following the chemical reaction below [9].



Thus, the model of this unit is based on a mass balance based on the stoichiometry of the reaction assuming 100% conversion. The bed can be regenerated using oxygen [9].



A.3 CO₂, NH₃ AND H₂O REMOVAL (PSA)

The flue gas from the gas turbine is to be used as heat source to produce steam for the steam turbine. Therefore, it is interesting that the stream has high temperature. CO₂ is removed from biogas using a packed bed of zeolite 5A operating at 25 °C and 4.5 bar. To secure continuous operation, two adsorbent beds operate in parallel so that while one is in adsorbent mode, the second one is under regeneration. We assume a recovery of 100% for NH₃ and H₂O (because of their low total quantities in the biogas, in general), 95% for CO₂ and 0% for any other gas of the mixture [3, 5].

A.4 BRAYTON CYCLE

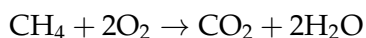
The process consists of a three stage polytropic compressor with intercooling. Each compressor is modelled assuming polytropic behavior using Eqs. A.20 - A.21 to compute the exit temperature and the power required for each stage. After each compression stage, intercooling is used to reduce the power input. The polytropic coefficient, k , is taken to be 1.4 based on an offline simulation using CHEMCAD®. The efficiency of the compressor is assumed to be 85% [8]. A maximum compression ratio of 40 for air is used, based on typical achievements [1]. The intercooling stage is modeled as simple energy balance to compute the cooling required to cool down the gas to the initial temperature of the previous compressor.

$$T_{out/compressor} = T_{in/compressor} + T_{in/compressor} \left(\left(\frac{P_{out/compressor}}{P_{in/compressor}} \right)^{\frac{z-1}{z}} - 1 \right) \frac{1}{\eta_c} \quad (\text{A.20})$$

Eq21

$$W_{compressor} = (F) \cdot \frac{R \cdot z \cdot (T_{in/compressor})}{((MW) \cdot (z - 1))} \frac{1}{\eta_c} \left(\left(\frac{P_{out/compressor}}{P_{in/compressor}} \right)^{\frac{z-1}{z}} - 1 \right) \quad (\text{A.21})$$

The combustion of the biogas, see reactions below, heats up the mixture. We use an excess of 20% of air with respect to the stoichiometry and assume 100% conversion of the reaction.



The material balance is based on the stoichiometry of the chemical reaction stated above and an energy balance is used to compute temperature of the gases exiting the gas turbine as given by Eq. A.22:

$$Q_{Furnace} = \sum_h \Delta H_{f,h}^{Furnace, GasTurb}(T) - \sum_h \Delta H_{f,h}^{Compres2,Furnace}(T) - \sum_h \Delta H_{f,h}^{Compres3,Furnace}(T) \quad (\text{A.22})$$

The hot flue gas is expanded in the gas turbine to generate power. Eq. A.21 is used to model the performance of the gas turbine. The polytropic coefficient is taken to be 1.3, also based on an offline simulation using CHEMCAD ®, with an efficiency of 85% [8]. Finally, the exhaust gas is cooled down and used to generate high pressure steam to be fed to the Rankine cycle.

A.5 RANKINE CYCLE

The steam is generated in a system of heat exchangers. Two alternatives are evaluated:

1. Only a fraction of the flue gas from the gas turbine is used to produce the high pressure steam fed to the steam turbine. The rest of the gas is used for the regeneration step.
2. The entire flue gas is used to heat up the saturated steam before feeding it to the high pressure turbine. Next, it is used to reheat the expanded steam before feeding it to the medium pressure turbine.

In the second body of the turbine, part of the steam is extracted at a medium pressure and it is used to heat up the condensate. The rest of the steam is finally expanded to an exhaust pressure, condensed and recycled. The flue gas is used for heating up and evaporating this stream. Due to the size of the plants and their typical location, a farm, it is expected that a lagoon is used to condensate the working fluid. Each unit is modeled using mass and energy balances as well as thermodynamic properties [7, 11].

The enthalpy and entropy of steam as a function of the temperature and pressure are correlated as in previous work [7, 11]. The equations can be found in the appendix below. Therefore, the stream exiting the first body can be calculated using Eqs. A.23-A.28, assuming an isentropic efficiency, η_s , of 0.9.

$$\eta_s = \frac{H_{steam}^{Turb1,HX5} - H_{steam,HX4,Turb1}}{H_{steam,isoentropy} - H_{steam}^{HX4,Turb1}} \quad (\text{A.23})$$

where:

$$H_{steam,isoentropy} = f(p_{Turb1,HX5}, T^*_{Turb1,HX5}) \quad (\text{A.24})$$

T^* represents the isentropic temperature after the expansion computed as follows:

$$\begin{aligned} s_{steam}^{HX4,Turb1} &= \\ f(p_{HX4,Turb1}, T_{HX4,Turb1}) &= f(p_{Turb1,HX5}, T^*_{Turb1,HX5}) \end{aligned} \quad (\text{A.25})$$

We make sure that the output of the turbine is superheated steam by maintaining its temperature above the one that corresponds to saturation for the pressure of the stream.

$$p_{turb,2} \cdot 760 = e^{\left(A_{H_2O} - \frac{B_{H_2O}}{(c_{H_2O} \cdot T_{turb,1,min})} \right)} \quad (\text{A.26})$$

$$T_{Turb,1,HX5} > T_{turb,1,min} \quad (\text{A.27})$$

The energy that is obtained in the steam expansion in the first turbine is given by Eq. A.28:

$$W_{Turbine1} = f c_{H_2O}^{HX4,Turb1} \cdot (H_{steam}^{HX4,Turb1} - H_{steam}^{Turb1,HX5}) \quad (\text{A.28})$$

The stream, as superheated vapor, is heated up again in HX5 using a fraction of the exhaust gas from the gas turbine, Eq. A.29, or the entire flow depending on the flowsheet configuration, Eq. A.30. Next, the superheated steam is fed to a second turbine. HX5 is modeled using Eq. A.29-A.31.

$$Q_{HX5} = f c_{H_2O}^{Turb1,HX5} \cdot (H_{steam}^{HX5,Turb2} - H_{steam}^{Turb1,HX5}) \quad (\text{A.29})$$

$$Q_{HX5} = -F^{Spl1,HX5} \cdot \int_{T_{Spl1,HX5}}^{T_{HX5,Mix1}} C p_{sat} dT \quad (\text{A.30})$$

$$Q_{HX5} = -F^{HX4,HX5} \cdot \int_{T_{(HX4,HX5)}}^{T_{HX5,Mix1}} C p_{sat} dT \quad (\text{A.31})$$

In the second turbine there is another expansion to a lower pressure. Part of the stream will be sent to HX7, while the rest is used in the third body of the turbine, where it is expanded to a pressure below atmosphere, see Eq. A.32; this pressure ranges from 0.05 bar to 0.31 bar in the literature [11]. The second and third bodies of the turbine are

calculated similarly to the first one, assuming 0.9 isentropic efficiency in all stages.

$$fc_{H_2O}^{HX5}, Turb2 = fc_{H_2O}^{Turb2}, HX7 + fc_{H_2O}^{Turb2}, Turb3 \quad (\text{A.32})$$

The stream extracted from the medium pressure turbine is sent to HX7, where it will be used to reheat the liquid obtained after condensing the exhaust of the third body of the turbine. The exhaust of the low pressure turbine is assumed to be saturated vapor. This stream is condensed in HX6:

$$Q_{(HX6)} = fc_{H_2O}^{Turb3}, HX6 \cdot (H_{liq}^{HX6, HX7} - H_{steam}^{Turb3, HX6}) \quad (\text{A.33})$$

This energy must be removed in the cooling system. We assume that a lagoon is used to cool down the water used to condense the saturated steam before reuse. This part is not included in the model. When mixing the exhaust of the second turbine with the compressed liquid from HX6, we must bear in mind that the outlet should be liquid since it is going to be compressed and heated up as a liquid in HX8. Eq. A.34 ensures this fact:

$$T_{HX7, HX8} \leq T_{turb, 2, min} \quad (\text{A.34})$$

BIBLIOGRAPHY

- [1] Jane's Aero-engines. *Jane's Information Group*, tech. rep. Sentinel House, 1997.
- [2] T. Al Seadi, D. Rutz, H. Prassl, M. Köttner, T. Finsterwalder, S. Volk, and R Janssen. *Biogas handbook*. English. 2008th ed. Denmark: Syddansk Universitet, 2008. ISBN: 978-87-992962-0-0.
- [3] Gas Processors Suppliers Association. *GPSA engineering data book*, 12th ed. Tech. rep. Gas Processors Suppliers Association, 2004.
- [4] Department for Environment Food and Rural Affairs (DEFRA). *Fertiliser Manual (RB209)*. <http://adlib.eversite.co.uk/adlib/defra/content.aspx?doc=262994&id=263068>. [Online; accessed 29-April-2017]. 2011.
- [5] Nexant Inc. *Equipment Design and Cost Estimation for Small Modular Biomass Systems, Synthesis Gas Cleanup, and Oxygen Separation Equipment. Task 2: Gas Cleanup Design and Cost Estimates – Black Liquor Gasification*. Tech. rep. National Renewable Energy Laboratory (NREL), 2006.

- [6] Prasad Kaparaju and Jukka Rintala. «Generation of heat and power from biogas for stationary applications: boilers, gas engines and turbines, combined heat and power (CHP) plants and fuel cells.» In: *The biogas handbook*. Elsevier, 2013, pp. 404–427.
- [7] Lidia Martín and Mariano Martín. «Optimal year-round operation of a concentrated solar energy plant in the south of Europe.» In: *Applied Thermal Engineering* 59.1-2 (2013), pp. 627–633.
- [8] M.J. Moran and H.N. Shapiro. *Fundamentals of Engineering Thermodynamics*. 5th ed. Wiley, 2003.
- [9] Eline Ryckebosch, Margriet Drouillon, and Han Vervaeren. «Techniques for transformation of biogas to biomethane.» In: *Biomass and bioenergy* 35.5 (2011), pp. 1633–1645.
- [10] R. Sinnott. «Coulson and Richardson's Chemical Engineering.» In: *Chemical engineering design* (1999).
- [11] M Vidal and M Martín. «Optimal coupling of biomass and solar energy for the production of electricity and chemicals.» In: *Comp. Chem. Eng* 72 (2015), pp. 273–283.

B

APPENDIX B: SUPPLEMENTARY INFORMATION OF CHAPTER 3

B.1 CATTLE ORGANIC WASTE COMPOSITION

To calculate the distribution functions of the different compounds of the cattle organic waste, 37 data sets for cattle organic waste compositions from 20 bibliographic references were evaluated. Table B.1 collects the main statistical parameters of the data, and Table B.2 shows the data obtained from literature.

Table B.1: Statistical summary of cattle organic waste composition. Data from [1, 3, 6–14, 16–18, 20–23, 25, 26].

	DM (% mass)	C (% mass)	Ca (% mass)	K (% mass)	N (% mass)	P (% mass)	$\frac{\text{Ca}^{2+}}{\text{Total Ca}}$	$\frac{\text{K}^+}{\text{Total K}}$	$\frac{\text{N-NH}_4^+}{\text{Total N}}$	$\frac{\text{P-PO}_4^{3-}}{\text{Total P}}$
count	36	6	9	12	35	24	1	1	31	13
mean	5.858	2.478	0.117	0.253	0.384	0.059	0.154	1.000	0.590	0.541
std	1.778	0.946	0.027	0.158	0.133	0.038	NaN	NaN	0.117	0.159
min	2.624	1.200	0.080	0.084	0.114	0.005	0.154	1.000	0.348	0.216
25.00%	4.610	1.719	0.100	0.148	0.299	0.032	0.154	1.000	0.516	0.421
50.00%	5.668	2.788	0.110	0.223	0.399	0.048	0.154	1.000	0.616	0.597
75.00%	7.362	3.194	0.129	0.276	0.449	0.080	0.154	1.000	0.666	0.671
max	9.200	3.400	0.165	0.635	0.789	0.164	0.154	1.000	0.820	0.700

Table B.2: Data obtained from literature.

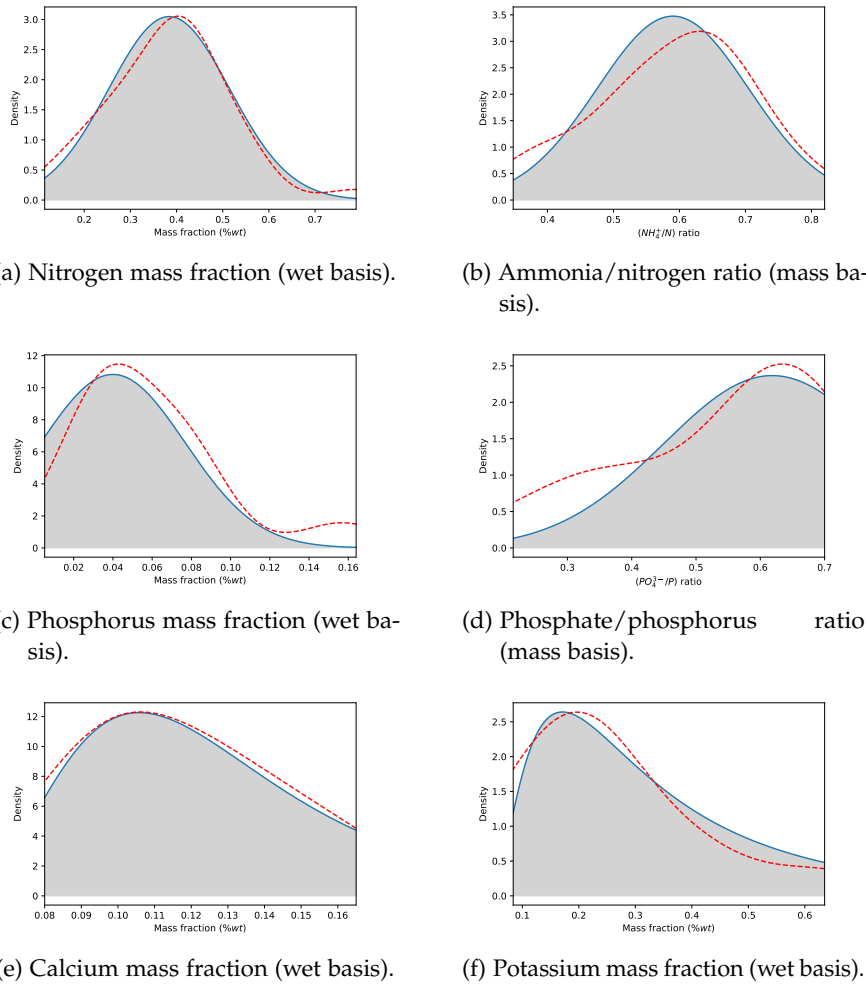


Figure B.1: Kernel density estimation (red dashed line) and probability density distribution (blue solid line) for the evaluated components in cattle organic waste.

B.2 DISTRIBUTION FUNCTIONS OF ELEMENTS FROM CATTLE WASTE

The kernel density estimation (KDE) method is used to fit the probability function to data distribution and to determine the probability density distributions of calcium, nitrogen, phosphorus, potassium, ammonia/total nitrogen, and phosphate/total phosphorus. As histograms, KDE is a non-parametric way to estimate the probability density function of a random variable. However, in the KDE method, kernels are functions associated with each data set. Thus, the unknown density function can be computed as the weighted sum of these functions [5].

The calculation procedure is divided into three steps. First, cattle organic waste composition data are collected from the literature. Second, the KDEs of all compounds are estimated, and finally, distribution

functions are fitted, using the kernel density estimations to validate the chosen distribution. The probability density distributions which best fit the data distribution are normal distribution functions for the distribution of nitrogen as in Figure B.1a, ammonia/total nitrogen molar ratio as observed in Figure B.1b, and phosphorus as shown in Figure B.1c. Lognormal distribution functions are the best fit for phosphate/total phosphorus molar ratio as in Figure B.1d, calcium, as shown in Figure B.1e, and potassium as observed in Figure B.1f.

B.3 THERMODYNAMIC MODELING OF THE CARBONATES SYSTEM

To calculate the total carbonate content, the concept of defining alkalinity will be used. The formal definition of total alkalinity is the capacity of a solution to buffer changes in pH that would make the solution more acidic. From the perspective of charge balance, total alkalinity can be considered as a measure of the number of protons that can be accepted by the proton acceptors present in the dissolution. Therefore, total alkalinity, TA , is calculated as the excess of proton acceptors over donors with respect to a chosen zero level of protons, as in Eq. B.1:

$$TA = \text{proton acceptors} - \text{proton donors} \quad (\text{B.1})$$

Note that the distribution of different species for various systems, such as carbonic acid and phosphoric acid, depend on pH, and the contribution of each species to alkalinity, is a function of its electrical charge. For our case, the chemical systems considered are water, carbonic acid, phosphoric acid, and ammonia systems

A zero level of protons is a reference system defined by choosing a certain chemical compound for each system at a certain pH selected arbitrarily. This reference chemical is the dominant species at the selected pH. The chemical species above this zero level of protons will be proton acceptors while species below this level will be proton donors in a determined chemical system. There is a standard defined by Dickson [4], where the reference pH value is set to 4.5 and chosen as the zero level of protons. For a more detailed discussion about alkalinity, we refer to Wolf-Gladrow et al. [24]. The dominant chemical substances for each system at the reference pH of 4.5 are H_2O , H_2CO_3 , $H_2PO_4^-$ and NH_4^+ . With these considerations, the proton donors and acceptors for each system are collected in Table B.3:

Table B.3: Proton donors and acceptors for each chemical system.

Chemical system	Proton donors	Proton acceptors
Water	$\{H^+\}$	$\{OH^-\}$
Carbonic acid	$\{H^+\}$	$\{HCO_3^-\}, 2 \cdot \{CO_3^{2-}\}$
Phosphoric acid	$\{H_3PO_4\}, \{H^+\}$	$\{HPO_4^{2-}\}, 2 \cdot \{PO_4^{3-}\}$
Ammonia system	$\{H^+\}$	$\{NH_3\}$

Therefore, the alkalinity due to carbonates, called carbonate alkalinity (Alk_{carb}), as described in Eq. B.2, can be calculated from total alkalinity value minus the alkalinity contribution of the other compounds, Eq. B.4. The activities of the chemical species from water,

phosphoric acid, and ammonia systems are obtained by solving the equilibrium and mass balance equations described previously.

The formulation of the alkalinity problem is described next. First, the alkalinity given in milligrams of CaCO_3 per liter is transformed into equivalents per liter by Eq. B.3 and the carbonate alkalinity is calculated through Eq. B.4.

$$\text{Alk}_{\text{carb}} = \{\text{HCO}_3^-\} + 2\{\text{CO}_3^{2-}\} \quad (\text{B.2})$$

$$\text{Alk} \left(\frac{\text{Eq}}{\text{L}} \right) = \frac{\text{mg}_{\text{CaCO}_3}}{\text{L}} \cdot \frac{1 \text{ g}}{1000 \text{ mg}} \cdot \frac{1 \text{ Eq}}{50 \text{ g}} \quad (\text{B.3})$$

$$\begin{aligned} \text{Alk}_{\text{carb}} = & \text{Alk} - \{\text{OH}^-\} - \{\text{HPO}_4^{2-}\} - 2\{\text{PO}_4^{3-}\} \\ & - \{\text{NH}_3\} + \{\text{H}_3\text{PO}_4\} + \{\text{H}^+\} \end{aligned} \quad (\text{B.4})$$

To compute the distribution of carbonate species, the fractions of each compound (α_{CO_2} , $\alpha_{\text{HCO}_3^-}$ and $\alpha_{\text{CO}_3^{2-}}$), which only depend on the pH, are calculated by employing Eqs. B.5 - B.7 [24]. As only HCO_3^- , and CO_3^{2-} contribute to alkalinity, the first one with one equivalent and the second one with two equivalents, as shown in Eq. B.2, it is necessary to add Eq. B.8. Because cattle waste has basic pH and the major species are HCO_3^- and CO_3^{2-} , it has been considered that total carbonates calculated in Eq. B.8, are equal to the sum of all carbonate species in the organic waste.

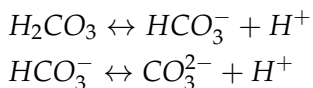
$$\alpha_{\text{CO}_2} = \frac{\{\text{H}^+\}^2}{\{\text{H}^+\}^2 + \{\text{H}^+\} K_{\text{sp}_{\text{H}_2\text{CO}_3}} + K_{\text{sp}_{\text{H}_2\text{CO}_3}} K_{\text{sp}_{\text{HCO}_3^-}}} \quad (\text{B.5})$$

$$\alpha_{\text{HCO}_3^-} = \frac{\{\text{H}^+\} K_{\text{sp}_{\text{H}_2\text{CO}_3}}}{\{\text{H}^+\}^2 + \{\text{H}^+\} K_{\text{sp}_{\text{H}_2\text{CO}_3}} + K_{\text{sp}_{\text{H}_2\text{CO}_3}} K_{\text{sp}_{\text{HCO}_3^-}}} \quad (\text{B.6})$$

$$\alpha_{\text{CO}_3^{2-}} = \frac{K_{\text{sp}_{\text{H}_2\text{CO}_3}} K_{\text{sp}_{\text{HCO}_3^-}}}{\{\text{H}^+\}^2 + \{\text{H}^+\} K_{\text{sp}_{\text{H}_2\text{CO}_3}} + K_{\text{sp}_{\text{H}_2\text{CO}_3}} K_{\text{sp}_{\text{HCO}_3^-}}} \quad (\text{B.7})$$

$$\text{Total carbonates} = \frac{\text{Alk}_{\text{carb}}}{\alpha_{\text{HCO}_3^-} + 2\alpha_{\text{CO}_3^{2-}}} \quad (\text{B.8})$$

Once the total carbonates concentration is known, the thermodynamic models for carbonate species existing in aqueous phase can be defined for the following species



Two elements are necessary to define the thermodynamic models for carbante species, the therodynamic equilibria defined by the Eq. B.9, computed using activity coefficients, and mass balance defined by Eq. B.11. Finally, solving the equations 2 to 11 the concentrations of the different carbonate species are determined. pK_{sp} values for all systems evaluated in this work are collected in Table B.4.

$$K_{sp} = \frac{\prod \{Products\}}{\prod \{Reactants\}} \quad (B.9)$$

$$[i]_{initial} = \sum_{products} [i]_{products} \quad (B.10)$$

$$i \in \{CO_3^{2-}\}$$

$$\text{Total carbonates} = [H_2CO_3] + [HCO_3^-] + [CO_3^{2-}] \quad (B.11)$$

Table B.4: pK_{sp} values for the considered aqueous phase chemical systems.

Name	Chemical system	pK_{sp}	Source
Ammonia	$NH_4^+ \leftrightarrow NH_3 + H^+$	9.2	[2]
Water	$H_2O \leftrightarrow OH^- + H^+$	14	[19]
	$H_3PO_4 \leftrightarrow H_2PO_4^- + H^+$	2.1	[15]
Phosphoric acid	$H_2PO_4^- \leftrightarrow HPO_4^{2-} + H^+$	7.2	[15]
	$HPO_4^{2-} \leftrightarrow PO_4^{3-} + H^+$	12.35	[15]
Carbonic acid	$H_2CO_3 \leftrightarrow HCO_3^- + H^+$	6.35	[19]
	$HCO_3^- \leftrightarrow CO_3^{2-} + H^+$	10.33	[19]

B.4 SURROGATE MODELS TO ESTIMATE THE FORMATION OF PRECIPITATES FROM LIVESTOCK ORGANIC WASTE

B.4.1 *Influence of magnesium*

B.4.1.1 *Influence of calcium*

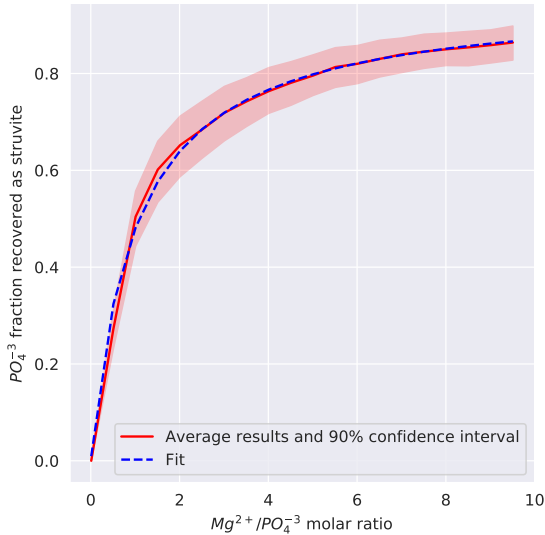
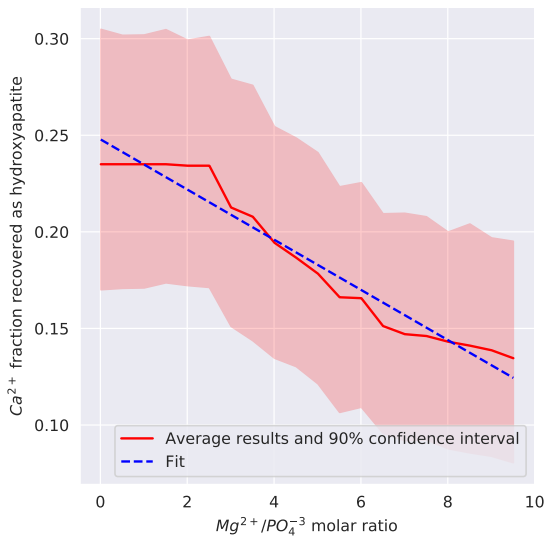
B.4.1.2 *Influence of alkalinity*

BIBLIOGRAPHY

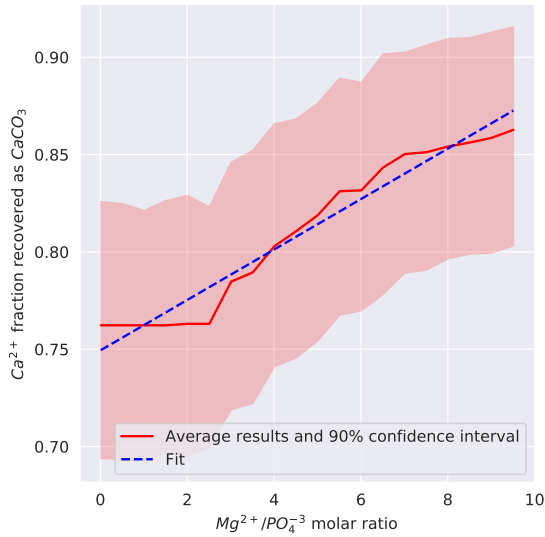
- [1] J.A. Alburquerque, C. de la Fuente, and M.P. Bernal. «Chemical properties of anaerobic digestates affecting C and N dynamics in amended soils.» In: *Agric. Ecosyst. Environ.* 160 (2012), pp. 15–22.
- [2] R. G. Bates and G. Pinching. «Acid dissociation constant of ammonium ion at 0–50 °C, and the base strength of ammonia.» In: *Journal of Research of the National Bureau of Standards* 42 (1949), pp. 419–430.
- [3] D. Bolzonella, F. Fatone, M. Gottardo, and N. Frison. «Nutrients recovery from anaerobic digestate of agro-waste: Techno-economic assessment of full scale applications.» In: *J. Environ. Manage.* 216 (2018), pp. 111–119.
- [4] A.G. Dickson. «An exact definition of total alkalinity and a procedure for the estimation of alkalinity and total inorganic carbon from titration data.» In: *Deep-Sea Res.* 28.6 (1981), pp. 609–623.
- [5] T. Duong. «An introduction to kernel density estimation.» In: *University of Western Australia* (2001).
- [6] K. Gell, J. van Groenigen, and M.L. Cayuela. «Residues of bioenergy production chains as soil amendments: Immediate and temporal phytotoxicity.» In: *J. Hazard. Mater.* 186 (2011), pp. 2017–2025.
- [7] H. Kirchmann and E. Witter. «Composition of fresh, aerobic and anaerobic farm animal dungs.» In: *Bioresour. Technol.* 40.2 (1992), pp. 137–142.
- [8] C. Ledda, A. Schievano, B. Scaglia, M. Rossoni, Acién Fernández F. G., and F. Adani. «Integration of microalgae production with anaerobic digestion of dairy cattle manure: an overall mass and energy balance of the process.» In: *J. Clean. Prod.* 112 (2016), pp. 103–112.
- [9] A.K. Løes, R. Pommeresche, and R. Khalil. *Effects of marble application to manure and anaerobic digestates.* Tech. rep. NORSØK, 2017.
- [10] J.H. Martin. *A Comparison of Dairy Cattle Manure Management with and without Anaerobic Digestion and Biogas Utilization.* Tech. rep. AgSTAR Program, U.S. Environmental Protection Agency, 2003.
- [11] K. Möller and T. Müller. «Effects of anaerobic digestion on digestate nutrient availability and crop growth: A review.» In: *Eng. Life Sci.* 12.3 (2012), pp. 242–257.

- [12] K. Möller, W. Stinner, A. Deuker, and G. Leithold. «Effects of different manuring systems with and without biogas digestion on nitrogen cycle and crop yield in mixed organic dairy farming.» In: *Nutr. Cycl. Agroecosyst.* 82.3 (2008), pp. 209–232.
- [13] V. Moset, D. Fontaine, and H.B. Møller. «Co-digestion of cattle manure and grass harvested with different technologies. Effect on methane yield, digestate composition and energy balance.» In: *Energy* 141 (2017), pp. 451–460.
- [14] A. Normak, J. Suurpere, K. Orupöld, E. Jõgi, and E. Kokin. «Simulation of anaerobic digestion of cattle manure.» In: *Agronomy Research Biosystem Engineering Special Issue* 1 (2012), pp. 167–174.
- [15] K. N. Ohlinger, T.M. Young, and E.D. Schroeder. «Predicting struvite formation in digestion.» In: *Wat. Res.* 32.12 (1998), pp. 3607–3614.
- [16] H. Rigby and S.R. Smith. *New Markets for Digestate from Anaerobic Digestion*. Tech. rep. WRAP (Waste and Resources Action Programme), 2011.
- [17] K. Risberg, H. Cederlund, M. Pell, V. Arthurson, and A. Schnürer. «Comparative characterization of digestate versus pig slurry and cow manure - Chemical composition and effects on soil microbial activity.» In: *Waste Manag.* 61 (2017), pp. 529–538.
- [18] M. Seppälä, V. Pyykkönen, A. Väisänen, and J. Rintala. «Biomethane production from maize and liquid cow manure - Effect of share of maize, post-methanation potential and digestate characteristics.» In: *Fuel* 107 (2013), pp. 209–216.
- [19] D.A. Skoog, D.M. West, F.J. Holler, and S.R Crouch. *Fundamentals of analytical chemistry*. Cengage Learning, 2014. ISBN: 9780495558286.
- [20] K. Smith, J. Grylls, P. Metcalfe, B. Jeffrey, and A. Sinclair. *Nutrient Value of Digestate from Farm-Based Biogas Plants in Scotland*. Tech. rep. Scottish Executive Environment and Rural Affairs Department, 2007.
- [21] P. Sørensen, P. Mejnertsen, and H.B. Møller. «Nitrogen fertilizer value of digestates from anaerobic digestion of animal manures and crops.» In: *NJF Report* 7.8 (2011), pp. 42–44.
- [22] M. Tampere and R. Viiralt. «The efficiency of biogas digestate on grassland compared to mineral fertilizer and cattle slurry.» In: *Research for Rural Development* 1 (2014), pp. 89–94.
- [23] J.J. Walsh, D.L. Jones, G. Edwards-Jones, and A.P. Williams. «Replacing inorganic fertilizer with anaerobic digestate may maintain agricultural productivity at less environmental cost.» In: *J. Plant. Nutr. Soil Sci.* 175.6 (2012), pp. 840–845.

- [24] D.A. Wolf-Gladrow, R.E. Zeebe, C. Klaas, A. Kötzinger, and A.G. Dickson. «Total alkalinity: The explicit conservative expression and its application to biogeochemical processes.» In: *Mar. Chem.* 106 (2007), pp. 287–300.
- [25] M. Xia, W. Tao, Z. Wang, and Y. Pei. «Treatment of anaerobically digested dairy manure in a two-stage biofiltration system.» In: *Water Sci. Technol.* 65.11 (2012), pp. 1975–1981.
- [26] Y. Zheng, L. Ke, D. Xia, Y. Zheng, Y. Wang, H. Li, and Q. Li. «Enhancement of digestates dewaterability by CTAB combined with CFA pretreatment.» In: *Sep. Purif. Technol.* 163 (2016), pp. 282–289.

(a) $x_{\text{struvite}}(\text{PO}_4^{3-})$ 

(b) Hydroxyapatite



(c) Calcium carbonate

Figure B.2: Evolution phosphorus as phosphate fraction recovered as struvite and calcium fraction recovered as precipitates along $\text{Mg}^{2+}/\text{PO}_4^{3-}$ molar ratio values considering 50 different composition data sets.

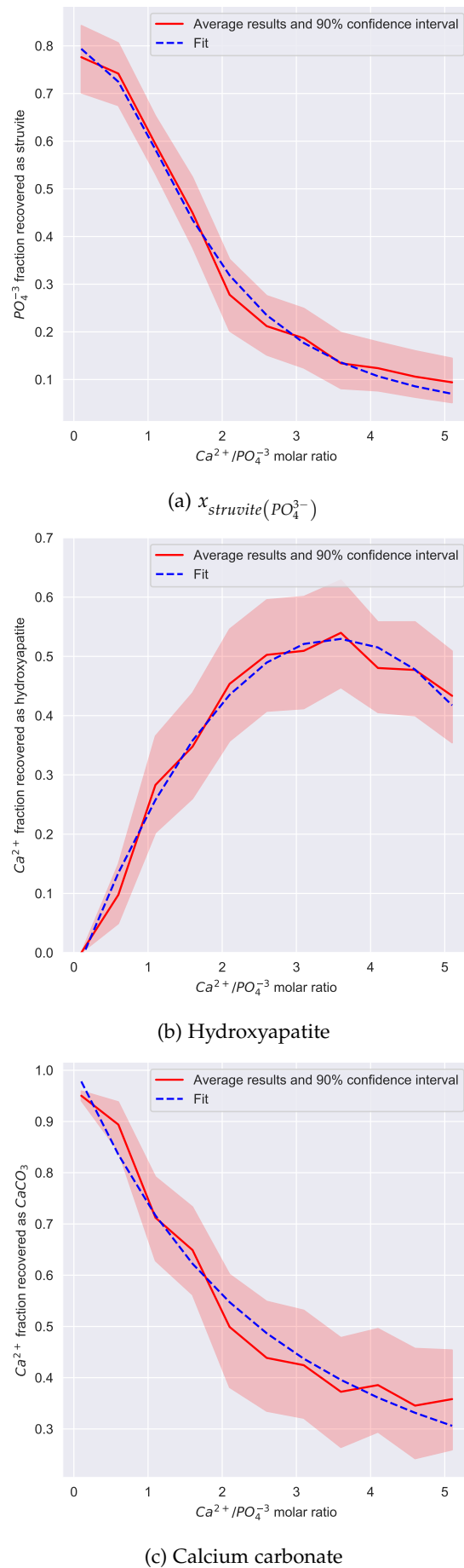
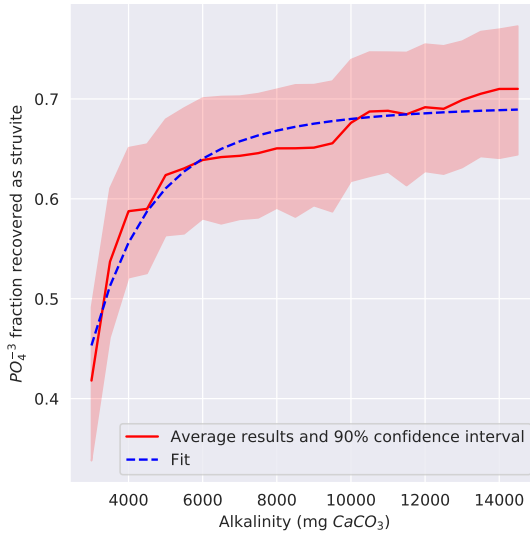
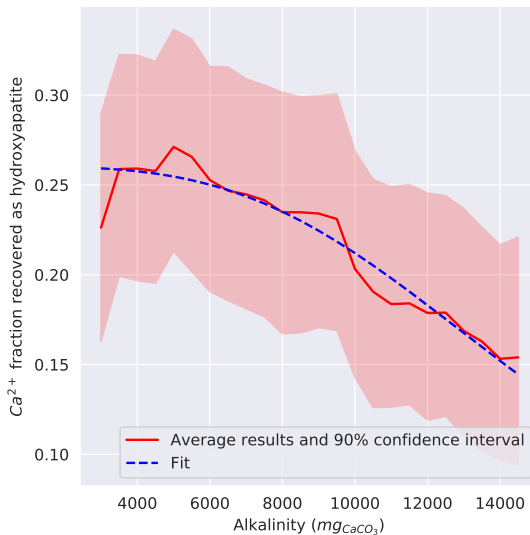
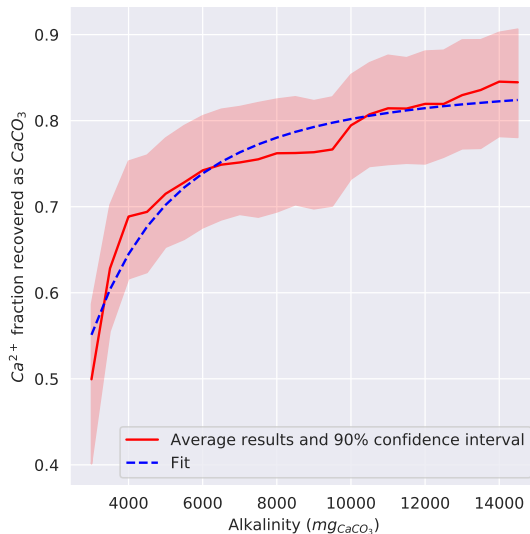


Figure B.3: Evolution of phosphorus as phosphate fraction recovered as struvite and calcium fraction recovered as precipitates along $\text{Ca}^{2+}/\text{PO}_4^{3-}$ molar ratio values considering 50 different composition data sets.

(a) $x_{\text{struvite}}(\text{PO}_4^{3-})$ 

(b) Hydroxyapatite



(c) Calcium carbonate

Figure B.4: Evolution of phosphorus as phosphate fraction recovered as struvite and calcium fraction recovered as precipitates among alkalinity values considering 50 different composition data sets.

C

APPENDIX C: SUPPLEMENTARY INFORMATION OF CHAPTER 4

C.1 BIOGAS PRODUCTION

D

APPENDIX D: SUPPLEMENTARY INFORMATION OF CHAPTER 6

D.1 BIOGAS PRODUCTION

APPENDIX E: SUPPLEMENTARY INFORMATION OF CHAPTER 7

E.1 LITERATURE REVIEW

The literature available referred to CO₂ capture is extensive, not only for combustion processes also for the particular case of biogas upgrading, there exists a lack of literature regarding the selection of the most appropriate biogas upgrading technology. It should be noted that the goal of this work it is not limited to the optimization the biogas production and upgrading processes, which it is implicitly done in the work, but the aim pursued is to determine the optimal biogas upgrading technology among the different feasible processes.

This lack in the literature was detected after a literature review, carried out with special emphasis in specific studies about biogas upgrading. On one hand, as a result of the literature review made, it could be concluded that the literature about reviews of biogas upgrading processes is extensive, even when only recent works are considered, as it is shown in Table E.1. On the other hand, just a few recent works are approaching to carry out a systematic comparison of the processes, such as the work of Collet et al. [6], where a comparison of several CO₂ capture technologies using experimental data from other studies is presented, but without integrating and optimizing the biogas production and upgrading processes, or the study of Vo et al. [30], where simulations of biogas upgrading processes limited to amine scrubbing and biological methanation are carried out, not including some essential upgrading technologies such as membranes or PSA. Other works, including but not limited to Capra et al. [5], Curto and Martín [7], and Gilassi et al. [13], determine the optimal biogas upgrading process but analyzing only one technology in each case (amines scrubbing, biogas methanation, and membrane separation). In the work presented, 5 technologies have been evaluated considering both heuristic and mathematical modelling stages (biogas methanation, water scrubbing, pressure swing adsorption systems, amines scrubbing, and membranes separation systems).

E.2 MODELLING APPROACH

E.2.1 *Amines*

The CO₂ absorption systems using amines typically operate at low temperatures, around 25-30 °C, and partial pressures above 0.05 bar,

Table E.1: Relevant literature for biogas upgrading.

Author	Study performed
Angelidaki et al. [2]	Review of biogas upgrading technologies
Awe et al. [3]	Review of biogas upgrading technologies
Bauer et al. [4]	Review of biogas upgrading technologies
Khan et al. [17]	Review of biogas upgrading technologies
Miltner, Makaruk, and Harasek [21]	Review of biogas upgrading technologies
Sun et al. [26]	Review of biogas upgrading technologies
Zhou, Chaemchuen, and Verpoort [35]	Review of biogas upgrading technologies
Collet et al. [6]	Techno-economic and life cycle assessment of biogas upgrading
Ferella et al. [9]	Techno-economic assessment of strategic plans for biogas upgrading plants
Toledo-Cervantes et al. [28]	Comparison of photosynthetic and physico-chemical biogas upgrading processes
Vo et al. [30]	Simulation of amine scrubbing and biological methanation
Capra et al. [5]	Optimal selection of amine scrubbing process for biogas upgrading
Curto and Martín [7]	Optimal selection of renewable biogas methanation processes
Filipetto et al. [12]	Optimal selection of membrane separation process for biogas upgrading
Gilassi et al. [13]	Optimal selection of membrane separation process for biogas upgrading
Morero, Gropelli, and Campanella [22]	Optimal selection of amine scrubbing process for biogas upgrading

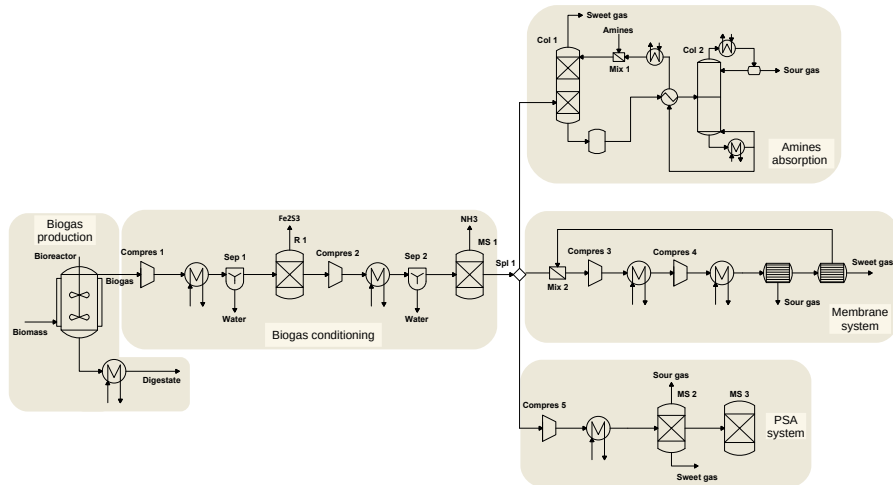


Figure E.1: Scheme of the proposed superstructure for biogas upgrading into biomethane.

reaching removal yields of 90%-95% [34]. In contrast to postcombustion gases, which contains large amounts of nitrogen from air, biogas is composed mainly by methane and CO₂, resulting in higher carbon dioxide partial pressures and in the need for lower operating pressures. CO₂ partial pressures above 0.1 bar have been assumed to secure high removal yields [34], resulting in the need to operate at total pressures around 1-1.5 bar to secure the appropriate CO₂ partial pressures [23, 33].

The total amount of solution of amines needed to absorb the CO₂ from the gas stream is calculated as a function of the amount of sour gases eliminated, Eq. E.1. According to GPSA [15], the concentration of solution and the correction factor (GPSA) depend on the amine used, as is shown in Table E.2. The flow of the amine solutions depends on their solubility. Thus, for a fixed removal ratio, the amines solution flow required changes from one to another. It is considered there is

no methane absorption in the amines flow, therefore all biomethane entering in the unit leaves the column and it is sent to storage.

$$fc_{amine} = \frac{MW_{amine}}{[amine]} \cdot \left(\frac{CO_{2eff} \cdot fc_{CO_2}}{MW_{CO_2}} \right) \cdot \left(\frac{1}{GPSA} \right) \quad (E.1)$$

The solution of amine used in column 1 comes from two sources, as shown in Eq. E.2, i.e., the amines from the regeneration column (column 2 in Figure 1), and some make-up solution to replace the amine losses with the gas outlet stream in the regeneration column. Additionally, to mix the two streams of amines at the same temperature, a heat exchanger is used to adjust the temperature of the amine flow stream which leaves the regeneration column to 25 °C.

$$fc_{amine} = fc_{recycled\ amine} + fc_{fresh\ amine} \quad (E.2)$$

The mixing of the two amines streams is assumed to be adiabatic. The energy balance to the heat exchanger is as follows, Eq. E.3.

$$Q = F_{amine} \cdot q_{heat,amine} \quad (E.3)$$

Where F_{amine} is referred to the total mass flow of the amines stream, and q_{amine} the heat flow ratio based on the rules of thumb reported by GPSA [15]. The values are collected in Table E.2.

The assumed CO₂ removal efficiency in the absorption column is 0.95, based on literature data [34]. The sour gas is absorbed by the amines in the absorption column, being withdrawn from the gas phase. The absorption is an exothermic process. Therefore, this energy is to be refrigerated, and the operation of the column is isothermal, Eq. E.4. The heats of reaction are shown in Table E.3.

$$Q_{Col1} = \Delta H_{react,amine} \cdot CO_{2eff} \cdot fc_{CO_2} \quad (E.4)$$

The biomethane leaves the column and it is sent to storage. On the other hand, the amine with the CO₂ absorbed is sent to the regeneration column (column 2). The solution is heated up before being fed to column 2 through the heat transfer from the amines stream leaving the reboiler of the regeneration column with the aim of improving the desorption process. Rules of thumb reported in the literature are used to compute the energy involved in the heat exchanger using Eq. E.6, considering the corresponding values of q_{amine} collected in Table E.3.

The operation of column 2 is also based on rules of thumb [14, 15] including the estimation of the energy consumption in the reboiler and the cooler refrigeration requirements. According to the literature, the inlet temperature to column 2, T_{Col2} , is equal to 93 °C, whereas

the temperature of the outlet amines stream, T_{bottom} , is equal to 125 °C, while at the condenser, the temperature, T_{top} , is equal to 54 °C. Thus, the energy balances of the stream entering column 2 are described in Eq. E.5.

$$\begin{aligned} Q_{Cond} &= F_{Cond} \cdot q_{Cond,amine} \\ Q_{Reb} &= F_{Reb} \cdot q_{Reb,amine} \end{aligned} \quad (\text{E.5})$$

From the reboiler, the regenerated amine is cooled down heating up the feed to the column, Eq. E.6.

$$Q_{Cooling} = F_{Cooling} \cdot q_{Cooling,amine} \quad (\text{E.6})$$

The gas leaving the regeneration column is saturated with the amines aqueous solution, producing the losses of amines which have to be replaced before being recirculated to the absorption column. In order to calculate these losses, humidification models are used. First, the saturation pressure of the amine solution is calculated, Eq. E.7. Then, the specific humidity of the gaseous stream is computed to determine the amount of amines solution accompanying the CO₂ gaseous stream which leaves the regeneration column, Eq. E.8, where the operating pressure of the regeneration column, P_{Col2} , is equal to 1.7 bar [14]. As an approximation, it is assumed that the amine solution behaves as water. The amount of amine lost with the sour gases is the one to be fed as fresh amine.

$$P_{amines\ solution} = \text{Exp} \left(A - \frac{B}{(C + T_{top})} \right) \quad (\text{E.7})$$

$$Y = \frac{MW_{Wa}}{MW_{outlet\ gas}} \cdot \frac{P_{amines\ solution}}{(P_{Col2} - P_{amines\ solution})} \quad (\text{E.8})$$

Three different amines are selected aiming a high selectivity, MEA, DEA, and MDEA. Table E.2 shows the parameters used in the amines absorption modelling for each amine considered [14, 15].

The biomethane production model through amines scrubbing includes the units described in sections ?? and E.2.1. The NLP problem consists of 288 equations and 953 variables per amine evaluated and is solved using a multistart initialization approach with CONOPT as the preferred solver where the main decision variable are the pressures temperatures and flow rates.

E.2.2 PSA

The stream of gases passes through the bed of zeolites and the carbon dioxide is captured by adsorption. The system consists of the compression train and the zeolite beds.

Table E.2: Amine properties for CO₂ capture GPSA [14, 15].

	MEA	DEA	MDEA
Gas pickup (mol/mol _{amine})	0.35	0.35-0.65	0.2-0.55
Solution concentration (wt %)	20	35	45
Heat of reaction (BTU/lb CO ₂)	620-700	580-650	570-600
GPSA	0.35	0.50	0.38
Density	1.01	1.05	1.05
Cost (EUR/kg)	1.30	1.32	3.09
Molecular weight	61	105	119

Table E.3: Amine regeneration heat loads GPSA [14].

	Duty (BTU/hr)
Reboiler	72000 GPM
Condenser	30000 GPM
Amine feed to distillation	45000 GPM
Amine cooler	15000 GPM

The adsorption capacity of the zeolites is directly related to the partial pressure of the CO₂. Therefore, a system of compressors with intermediate cooling is implemented to determine the optimal operating pressure. As it is described previously, the compressors are modelled assuming polytropic behavior, with a polytropic coefficient z of 1.4 and an efficiency of the compression stages of 0.85, Eq. E.9.

$$T_{out/compressor} = T_{in/compressor} + T_{in/compressor} \left(\left(\frac{P_{out/compressor}}{P_{in/compressor}} \right)^{\frac{z-1}{z}} - 1 \right) \frac{1}{\eta_c}$$

$$W_{(Compressor)} = (F) \cdot \frac{R \cdot z \cdot (T_{in/compressor})}{((Mw) \cdot (z-1))} \frac{1}{\eta_c} \left(\left(\frac{P_{out/compressor}}{P_{in/compressor}} \right)^{\frac{z-1}{z}} - 1 \right) \quad (E.9)$$

The removal ratio is given by the breakthrough curve of the adsorbent bed. Based on experimental data [16] for adsorption stages below 20 min, the CO₂ removal yield of the PSA system is assumed to be 98%, containing below 2% CO₂ at the outlet stream, [10]. The mass balance at the bed is as shown in Eq. E.10.

CO_2 stream:

$$\begin{aligned} f_{\text{CO}_2}|_{\text{out}} &= \eta f_{\text{CO}_2}|_{\text{in}} \\ f_{\text{CH}_4}|_{\text{out}} &= 0.02 \cdot f_{\text{CH}_4}|_{\text{in}} \end{aligned} \quad (\text{E.10})$$

CH_4 stream:

$$\begin{aligned} f_{\text{CO}_2}|_{\text{out}} &= (1 - \eta) f_{\text{CO}_2}|_{\text{in}} \\ f_{\text{CH}_4}|_{\text{out}} &= 0.98 \cdot f_{\text{CH}_4}|_{\text{in}} \end{aligned}$$

To compute the mass of bed the adsorption capacity of the bed is evaluated. Based on experimental data, the Langmuir isotherm is the adsorption model considered for this process, Eq. E.11, since this is the one that best fits the performance of the zeolite 13X - CO_2 system [16].

$$q = \frac{q_m \cdot K \cdot P_{\text{CO}_2}}{1 + K \cdot P_{\text{CO}_2}} \quad (\text{E.11})$$

Where the parameters q_m and K depend on the adsorbent material. Considering zeolite 13X, the effect of the operating temperature, within the range of 25 °C-60 °C, for both parameters can be correlated using data available in the literature, Eq. E.12a [16].

$$\begin{aligned} q_m &= -3.15551 \cdot 10^{-2}T(\text{°C}) + 5.02915 \\ K &= (1.63070 \cdot 10^{-3}T(\text{°C}))^2 - 3.68662 \cdot 10^{-1}T(\text{°C}) + 27.3737 \end{aligned} \quad (\text{E.12a})$$

$$\begin{aligned} q_m &= -1.8235510^{-2}T(\text{°C}) + 3.72021 \\ K &= 1.6307010^{-3}T(\text{°C})^2 - 3.6866210^{-1}T(\text{°C}) + 27.3737 \end{aligned} \quad (\text{E.12b})$$

As result of the breakthrough curve for the zeolite 13X – carbon dioxide system, the operating time must be below 20 min so that the exit gas (methane) contains only traces of CO_2 . Similarly, correlations are developed for zeolite 4A, Eq. E.12b. The operating time of zeolite 4A must be below 20 min [16]. Note that the expression for the computing of the constant K in the Langmuir correlation is the same for both adsorbents evaluated.

However, the adsorption capacity decays cycle after cycle until it stabilizes around 65% of the initial capacity computed by Eq. E.13 [16]. Therefore, a corrected value for q is applied to compute the amount of zeolite used in the PSA system, as it can be shown in Eq. 14, where the CO_2 removal yield of the PSA system, is assumed to be 98%, containing below 2% CO_2 at the outlet stream [10], and τ is equal to 20 min, based on the results of [16]. Furthermore, a lifetime of the zeolites bed of 5 years has been considered based on data reported by Xiao, G.,

Webley, P., Hoadley, A., Ho, M., Wiley, D. [32]. Thus for the cost, we considered that over the 20 years life time of the plant, 5 beds will be used.

$$m_{Zeolite} = \frac{1}{q \cdot 0.65} \frac{f_{CO_2} \cdot 1000}{MW_{(CO_2)}} \eta \cdot \tau \quad (\text{E.13})$$

In the case of the PSA system, the objective function is shown in Eq. E.14. To estimate the cost of the PSA system, Eq. E.15, it is assumed that the zeolite bed loses efficiency over time, resulting in a lifetime of 5 years before it needs to be replaced [32]. As the plant life is considered 20 years, the zeolites bed must be replaced 4 times during the plant life, N_{Cycle} .

$$\text{Profit} = \text{BioCH}_4 - \text{Cost}_{\text{Zeolite system}} \quad (\text{E.14})$$

$$\text{Cost}_{\text{Zeolite system}} = C_{\text{Electricity}} \cdot W_{\text{Compressor}} + \frac{1}{K} M_{\text{Zeolite}} \cdot C_{\text{Zeolite}} \cdot N_{\text{Cycle}} \quad (\text{E.15})$$

The cost of the zeolites considered is 5 USD/kg for both zeolite 13X and zeolite 4A [32].

The production of biomethane through pressure swing adsorption includes the units described in sections ?? and E.2.2 consisting of an NLP problem of 283 equations and 828 variables that is solved similarly as in the case of the selection of amines where the main decision variables are the operating pressure of the adsorption tower and the size of the bed.

E.2.3 Membranes

The membrane system considered is dual-stage membrane systems with single compression stage before the membrane system and no recompression stage between membrane units, have been deemed as the most economic under a wide range of feed compositions [18]. The compressor is modelled as presented above, assuming polytropic compression of the gas, Eq. E.9. Each membrane module is modelled using mass balances, considering the permeate and retentate streams, Eqs. E.16 and E.17, and the flux of the gases through the membrane, that is a function of the concentration gradient between both sides of the membrane, Eq. E.19 [11]. The flux is the parameter which allows computing the area of the membrane, as it is shown in Eq. E.18, based on the permeability of the membrane, Eq. E.21. As the driving force in the membrane separation process is the concentration gradient, the removal of CO₂ results in a change in the composition of the stream along the membrane, leading to a change in the driving force which

controls the process. Therefore, an average molar fraction between the feed and the retentate composition is used to compute the separation driving force, Eq. E.20.

$$F_{feed} = F_{permeate} + F_{retentate} \quad (\text{E.16})$$

$$F_{feed} \cdot y_{i,feed} = F_{permeate} \cdot y_{i,permeate} + F_{retentate} \cdot y_{i,retentate}; i \in (CO_2, CH_4) \quad (\text{E.17})$$

$$J_i = \frac{F_{permeate} \cdot y_{i,permeate}}{A_{membrane}}; i \in (CO_2, CH_4) \quad (\text{E.18})$$

$$J_i = \varepsilon_i [y_{feedside} \cdot P_{feed} - y_{i,permeate} \cdot P_{Permeate}]; i \in (CO_2, CH_4) \quad (\text{E.19})$$

$$y_{feedside} = \frac{y_{i,feed} - y_{i,retentate}}{\ln \left(\frac{y_{i,feed}}{y_{i,retentate}} \right)}; i \in (CO_2, CH_4) \quad (\text{E.20})$$

$$\varepsilon_i = \frac{Perm_i}{\delta}; i \in (CO_2, CH_4) \quad (\text{E.21})$$

Where δ is the membrane thickness, and $Perm_i$ the permeability of the component i . The usual membrane thickness for industrial units is equal to 30 nm. Three different membrane materials are selected aiming a large CO_2 permeability, low methane permeability, and therefore, high selectivity; cellulose acetate, polyamide, and polycarbonate. Table E.4 shows the permeabilities for each membrane material considered in the model at 25 °C [31]. The solution of the optimization problem will yield intermediate conditions to assure natural gas composition of the biomethane.

Table E.4: Gases permeability Vrbová and Ciahotnyý [31].

Permeability (Barrer)		
Polymer	CH ₄	CO ₂
Cellulose acetate	0.21	6.30
Polycarbonate	0.13	4.23
Polyimide	0.25	10.7

Finally, the simplified profit objective function for the membrane separation system, Eq. E.22, considers cost of the gas compression and the amortization of the investment costs of the membranes, Eq. E.23.

$$Profit = BioCH_4 - Cost_{Membrane\ system} \quad (E.22)$$

Eq21

$$\begin{aligned} Cost_{Membrane\ system} = \\ C_{Electricity} \cdot W_{Compressor} + \frac{1}{K} \cdot C_{Membrane} \cdot \frac{1}{Lf} \cdot N_{Membranes} \left(\sum_{i \in stages} Area_i \right) \end{aligned} \quad (E.23)$$

A value of 50 USD/m² will be used based on the literature [18]. Considering the plant life equal to 20 years, the membranes with a typical lifetime of 4 years must be replaced 5 times during the plant life, $N_{Membranes}$ [25].

The biogas production and upgrading considering a membranes separation system is formulated as an NLP problem considering the units described in sections ?? and E.2.3 consisting of 299 equations and 869 variables for each material evaluated where the major decision variables are the flows, operating pressures, temperatures and the area required by the membrane units.

E.3 ECONOMIC EVALUATION

The evaluation of the cost for biomethane production is also estimated from different wastes. The production and investment costs are estimated. The CAPEX, or investment cost, is estimated based on Towler and Sinnott [29] that presents a factorial method. This method estimates the CAPEX usinf as reference the cost of all the major units of the flowsheet.

The sizing of all the units involved in the flowsheet, see Figure 2, is carried out following the method presented in Martín and Grossmann [20], and updated by Almena and Martín [1]. However, the following considerations for some specific units have been assumed:

- For the digester cost, assumed to be 365 EUR/m³ [27].
- The cost estimation of the columns for the amines is carried out using the rules reported in GPSA [15]. The diameter for the amine contactor can be estimated as given in Eq. E.24.

$$D_C = 44 \sqrt{\frac{F_{gas}(\text{MMscfd})}{P(\text{psia})}} \quad (E.24)$$

While the diameter of the regenerator column can be estimated as given in Eq. E.25.

$$D_R = 3.0 \sqrt{F_{amine} (\text{gal/min})} \quad (\text{E.25})$$

We use the same factors as presented in Davis and Martín [8] to estimate the investment, CAPEX, of the facility for further comparison with other renewable based methane production processes. The costs for piping, isolation, instrumentation, and utilities infrastructure are estimated with respect to the equipment cost as 20%, 15%, 20% and 10% of its value respectively. Land and buildings costs are estimated to be 8 M EUR. These items add up to the fixed cost. The fees represent 1% of the fixed cost, other administrative expenses and overheads, and the plant layout represent 10% of the direct costs (fees plus fixed capital) and 5% of the fixed cost, respectively. Finally, the plant start-up cost represents 5% of the investment.

Furthermore, the production costs of biomethane are estimated using also the factorial method with the coefficients presented and validated in Davis and Martín [8]. For the average annual cost, the labour costs (0.5% of investment), equipment maintenance and raw materials (1% of fix costs), amortization (linear with time in 20 years), taxes (0.5% of investment), overheads (1% of investment), and administration (5% of labour, equipment maintenance, amortization, taxes and overheads) are considered. The utilities, particularly cooling water, power, and steam, are taken from the mass and energy balances performed in the superstructure model. Heat integration is carried out to reduce the utilities consumption. The cost of electricity is 0.06 EUR/kWh. The hot compressed gas is used to evaporate the water and ammonia to prepare the digestate to be sold as fertilizer. However, the credit for the digestate to be used as fertilizer is difficult to be estimated. It depends on the market that typically is saturated. Although the cost is around 0.48 EUR/kg, only a fraction is typically obtained. To be conservative, a value of one third of this one is assumed to calculate the benefits received by the sold of the digestate produced [19]. In addition, the cost of the digestate for the methane to be competitive with other resources, targeting 5 EUR/MMBTU (0.17 EUR/Nm³), is computed.

E.4 SCALING-UP STUDY

The scaling-up study, based on the previous work of Sánchez and Martín [24], is performed in the following stages. Firstly, the capital cost of the different units is correlated as a function of a design variable, such as the membrane area for membranes systems or the column sizes in function of the flow processed. This variable will be denoted as scaling variable. The scaling variable of each equipment is directly related to the processing capacity of the facility studied through the mass or energy flows involved in that particular unit. The limitations

in the size of equipment are considered in the scaling-up study. When an equipment excess the size defined by the rules of thumb, that unit is duplicated, affecting to the cost estimation. In a second stage, after defined the scaling variables for all units and the relation between these units, the mass and energy flows and the processing capacity of the facility, different capacities are evaluated, calculating the mas and energy balances, and estimating the sizes of the equipment, and the number of units in case some equipment needs to be duplicated. In a third stage, the capital and operating costs are estimated considering the equipment sizes and number of unit of each equipment using the factorial method presented in Towler and Sinnott [29] and the estimation of the unit costs presented in Almena and Martín [1].

BIBLIOGRAPHY

- [1] Alberto Almena and Mariano Martín. «Technoeconomic analysis of the production of epichlorohydrin from glycerol.» In: *Industrial & Engineering Chemistry Research* 55.12 (2016), pp. 3226–3238.
- [2] Irini Angelidaki, Laura Treu, Panagiotis Tsapekos, Gang Luo, Stefano Campanaro, Henrik Wenzel, and Panagiotis G Kougias. «Biogas upgrading and utilization: Current status and perspectives.» In: *Biotechnology advances* 36.2 (2018), pp. 452–466.
- [3] Olumide Wesley Awe, Yaqian Zhao, Ange Nzihou, Doan Pham Minh, and Nathalie Lyczko. «A review of biogas utilisation, purification and upgrading technologies.» In: *Waste and Biomass Valorization* 8.2 (2017), pp. 267–283.
- [4] Fredric Bauer, Christian Hulteberg, Tobias Persson, and Daniel Tamm. *Biogas upgrading-Review of commercial technologies*. Tech. rep. Svenskt Gastekniskt Center AB, 2013.
- [5] Federico Capra, Federico Fettarappa, Francesco Magli, Manuele Gatti, and Emanuele Martelli. «Biogas upgrading by amine scrubbing: solvent comparison between MDEA and MDEA/MEA blend.» In: *Energy Procedia* 148 (2018), pp. 970–977.
- [6] Pierre Collet, Eglantine Flottes, Alain Favre, Ludovic Raynal, Hélène Pierre, Sandra Capela, and Carlos Peregrina. «Techno-economic and Life Cycle Assessment of methane production via biogas upgrading and power to gas technology.» In: *Applied energy* 192 (2017), pp. 282–295.
- [7] Diego Curto and Mariano Martín. «Renewable based biogas upgrading.» In: *Journal of Cleaner Production* 224 (2019), pp. 50–59.

- [8] William Davis and Mariano Martín. «Optimal year-round operation for methane production from CO₂ and water using wind energy.» In: *Energy* 69 (2014), pp. 497–505.
- [9] Francesco Ferella, Federica Cucchiella, Idiano D'Adamo, and Katia Gallucci. «A techno-economic assessment of biogas upgrading in a developed market.» In: *Journal of Cleaner Production* 210 (2019), pp. 945–957.
- [10] Francesco Ferella, Alessandro Puca, Giuliana Taglieri, Leucio Rossi, and Katia Gallucci. «Separation of carbon dioxide for biogas upgrading to biomethane.» In: *Journal of Cleaner Production* 164 (2017), pp. 1205–1218.
- [11] D. Fernandes Rodrigues. «Model Development of a Membrane Gas Permeation Unit for the Separation of Hydrogen and Carbon Dioxide.» MA thesis. Instituto Superior Técnico, Lisbon, 2009.
- [12] Diego Filipetto, Federico Capra, Francesco Magli, Manuele Gatti, and Emanuele Martelli. «Optimization of semi-permeable membrane systems for biogas upgrading.» In: *Computer Aided Chemical Engineering*. Vol. 46. Elsevier, 2019, pp. 1693–1698.
- [13] Sina Gilassi, Seyed Mohammad Taghavi, Denis Rodrigue, and Serge Kaliaguine. «Optimizing membrane module for biogas separation.» In: *International Journal of Greenhouse Gas Control* 83 (2019), pp. 195–207.
- [14] GPSA. *GPSA engineering data book, 12th ed.* Tech. rep. Gas Processors Suppliers Association, 2004.
- [15] GPSA. *GPSA engineering data book, 13th ed.* Tech. rep. Gas Processors Suppliers Association, 2012.
- [16] Lalhmingsanga Hauchhum and Pinakeswar Mahanta. «Carbon dioxide adsorption on zeolites and activated carbon by pressure swing adsorption in a fixed bed.» In: *International Journal of Energy and Environmental Engineering* 5.4 (2014), pp. 349–356.
- [17] Imran Ullah Khan, Mohd Hafiz Dzarfan Othman, Haslenda Hashim, Takeshi Matsuura, AF Ismail, M Rezaei-DashtArzhandi, and I Wan Azelee. «Biogas as a renewable energy fuel—A review of biogas upgrading, utilisation and storage.» In: *Energy Conversion and Management* 150 (2017), pp. 277–294.
- [18] Minsoo Kim, Sunghoon Kim, and Jiyoung Kim. «Optimization-based approach for design and integration of carbon dioxide separation processes using membrane technology.» In: *Energy Procedia* 136 (2017), pp. 336–341.
- [19] Erick León and Mariano Martín. «Optimal production of power in a combined cycle from manure based biogas.» In: *Energy Conversion and Management* 114 (2016), pp. 89–99.

- [20] Mariano Martín and Ignacio E Grossmann. «Energy optimization of hydrogen production from lignocellulosic biomass.» In: *Computers & chemical engineering* 35.9 (2011), pp. 1798–1806.
- [21] Martin Miltner, Alexander Makaruk, and Michael Harasek. «Review on available biogas upgrading technologies and innovations towards advanced solutions.» In: *Journal of Cleaner Production* 161 (2017), pp. 1329–1337.
- [22] Betzabet Morero, Eduardo S Gropelli, and Enrique A Campanella. «Evaluation of biogas upgrading technologies using a response surface methodology for process simulation.» In: *Journal of cleaner production* 141 (2017), pp. 978–988.
- [23] K Movagharnejad and M Akbari. «Simulation of CO₂ capture process.» In: *International Journal of Chemical and Molecular Engineering* 5.10 (2011), pp. 843–847.
- [24] Antonio Sánchez and Mariano Martín. «Scale up and scale down issues of renewable ammonia plants: Towards modular design.» In: *Sustainable Production and Consumption* 16 (2018), pp. 176–192.
- [25] Marco Scholz, Michael Alders, Theresa Lohaus, and Matthias Wessling. «Structural optimization of membrane-based biogas upgrading processes.» In: *Journal of membrane science* 474 (2015), pp. 1–10.
- [26] Qie Sun, Hailong Li, Jinying Yan, Longcheng Liu, Zhixin Yu, and Xinhai Yu. «Selection of appropriate biogas upgrading technology-a review of biogas cleaning, upgrading and utilisation.» In: *Renewable and Sustainable Energy Reviews* 51 (2015), pp. 521–532.
- [27] Manuel R Taifouris and Mariano Martin. «Multiscale scheme for the optimal use of residues for the production of biogas across Castile and Leon.» In: *Journal of cleaner production* 185 (2018), pp. 239–251.
- [28] Alma Toledo-Cervantes, José M Estrada, Raquel Lebrero, and Raúl Muñoz. «A comparative analysis of biogas upgrading technologies: Photosynthetic vs physical/chemical processes.» In: *Algal research* 25 (2017), pp. 237–243.
- [29] Gavin Towler and Ray Sinnott. *Chemical engineering design*. 5th ed. Elsevier, 2009.
- [30] Truc TQ Vo, David M Wall, Denis Ring, Karthik Rajendran, and Jerry D Murphy. «Techno-economic analysis of biogas upgrading via amine scrubber, carbon capture and ex-situ methanation.» In: *Applied energy* 212 (2018), pp. 1191–1202.
- [31] Veronika Vrbová and Karel Ciahotnyý. «Upgrading biogas to biomethane using membrane separation.» In: *Energy & Fuels* 31.9 (2017), pp. 9393–9401.

- [32] Xiao, G., Webley, P., Hoadley, A., Ho, M., Wiley, D. *Low Cost Hybrid Capture Technology Development: Final Report. Ref No: 3-0510-0046.* Tech. rep. Cooperative Research Centre for Greenhouse Gas Technologies. CO2CRC Publication, Canberra, Australia., 2013.
- [33] Boyang Xue, Yanmei Yu, Jian Chen, Xiaobo Luo, and Meihong Wang. «A comparative study of MEA and DEA for post-combustion CO₂ capture with different process configurations.» In: *International Journal of Coal Science & Technology* 4.1 (2017), pp. 15–24.
- [34] Ying Zhang and Chau-Chyun Chen. «Modeling CO₂ absorption and desorption by aqueous monoethanolamine solution with Aspen rate-based model.» In: *Energy Procedia* 37 (2013), pp. 1584–1596.
- [35] Kui Zhou, Somboon Chaemchuen, and Francis Verpoort. «Alternative materials in technologies for Biogas upgrading via CO₂ capture.» In: *Renewable and sustainable energy reviews* 79 (2017), pp. 1414–1441.